Heliyon 10 (2024) e35771

Contents lists available at ScienceDirect

Heliyon

journal homepage: www.cell.com/heliyon

Research article

A Fractional Order-Kepler Optimization Algorithm (FO-KOA) for single and double-diode parameters PV cell extraction

Sultan Hassan Hakmi [a], Hashim Alnami [a], Ahmed Ginidi [b], Abdullah Shaheen [b,**], Thamer A.H. Alghamdi [c,d,*]

[a] Department of Electrical and Electronic Engineering, College of Engineering and Computer Science, Jazan University, P.O. Box114, Jazan, 45142, Saudi Arabia
[b] Department of Electrical Engineering, Faculty of Engineering, Suez University, P.O. Box: 43221, Suez, Egypt
[c] Wolfson Centre for Magnetics, School of Engineering, Cardiff University, Cardiff, CF24 3AA, UK
[d] Electrical Engineering Department, School of Engineering, Al-Baha University, Al-Baha, 65779, Saudi Arabia

ARTICLE INFO

Keywords:
Kepler optimization algorithm
Single-diode model
Double-diode model
Parameters PV cell extraction

ABSTRACT

The primary objective of this study is to investigate the effects of the Fractional Order Kepler Optimization Algorithm (FO-KOA) on photovoltaic (PV) module feature identification in solar systems. Leveraging the strengths of the original KOA, FO-KOA introduces fractional order elements and a Local Escaping Approach (LEA) to enhance search efficiency and prevent premature convergence. The FO element provides effective information and past expertise sharing amongst the participants to avoid premature converging. Additionally, LEA is incorporated to boost the search procedure by evading local optimization. The single-diode-model (SDM) and Double-diode-model (DDM) are two different equivalent circuits that are used for obtaining the unidentified parameters of the PV. Applied to KC-200, Ultra-Power-85, and SP-70 PV modules, FO-KOA is compared to the original KOA technique and contemporary algorithms. Simulation results demonstrate FO-KOA's remarkable average improvement rates, showcasing its significant advantages and robustness over earlier reported methods. The proposed FO-KOA demonstrates exceptional performance, outperforming existing algorithms by 94.42 %–99.73 % in optimizing PV cell parameter extraction, particularly for the KC200GT module, showcasing consistent superiority and robustness. Also, the proposed FO-KOA is validated of on SDM and DDM for the well-known RTC France PV cell.

1. Introduction

The sun became the initial source of energy to produce heat and light, demonstrating the beginning of energy on Earth. The discovery of fire caused a revolution afterward; it was utilized for a variety of purposes such as cooking and as a source of heat and light as well. An industrial revolution was sparked by the discovery of fossil fuels, whose production from 1800 to 2009 averaged 93.467 million tonnes of oil equivalent each decade. The most prevalent fossil fuels are oil, coal, and natural gas, which when burned produce

* Corresponding author. Wolfson Centre for Magnetics, School of Engineering, Cardiff University, Cardiff, CF24 3AA, UK.
** Corresponding author.
E-mail addresses: shhakmi@jazanu.edu.sa (S. Hassan Hakmi), halnami@jazanu.edu.sa (H. Alnami), ahmed.ginidi@eng.suezuni.edu.eg (A. Ginidi), abdullah.mohamed.eng19@suezuni.edu.eg (A. Shaheen), AlghamdiT1@cardiff.ac.uk, thameraladnan@bu.edu.sa (T.A.H. Alghamdi).

https://doi.org/10.1016/j.heliyon.2024.e35771
Received 1 January 2024; Received in revised form 12 July 2024; Accepted 2 August 2024
Available online 5 August 2024
2405-8440/© 2024 The Authors. Published by Elsevier Ltd. This is an open access article under the CC BY-NC license (http://creativecommons.org/licenses/by-nc/4.0/).

the hazardous gas carbon dioxide (CO_2), with global CO_2 emissions from 1965 to 2021 with a total of 33884.06 (Metric tons of CO_2) $MTCO_2$. As the demand for clean and renewable energy continues to rise, the integration of distributed generation systems, particularly photovoltaic (PV) sources, into distribution systems has gained significant attention [1].

The single-diode-model (SDM) [2] and double-diode-model (DDM) [3] are just some of the examples of the multiple electrical models that have been studied in the literature. They will all be discussed in more detail in the following section. The primary problem is resolving the nonlinear equation provided by those models and figuring out its unidentified parameters; there are various methods of various kinds in the literature. There are analytical methods for figuring out the unknown parameters that rely on mathematical formulae [4]. The various techniques for accurately obtaining the evaluation parameters for PV models can be roughly categorized into analytical methods and Natural-inspired metaheuristics. The Newton-Raphson [5] and the Lambert W function [6] are examples of analytical methods. Natural-inspired metaheuristics (NiMH) are similar to a black box without any limits on the issue formulation, which enables them to successfully solve optimization and evaluation problems. This gives NiMH certain advantages over other approaches. NiMH has applications in numerous fields. Therefore, in recent years, researchers have utilized a variety of NiMH to address the parametric issues associated with solar PV cell models [7].

The modeling and performance forecasting in renewable energy technologies greatly benefit from the integration of artificial intelligence (AI) [8]. It plays a pivotal role in PV systems by leveraging its modeling and performance forecasting capabilities. Its applications range from optimizing energy generation and consumption to predictive maintenance, fault detection, and grid integration [9,10]. The integration of AI empowers stakeholders to make data-driven decisions and drives continuous advancements in PV technology, ultimately enhancing the efficiency, reliability, and sustainability of PV systems [11].

An enhanced augmented mutation Harris Hawk Optimizer (AMHHO) was proposed by Ridha et al. [12] to produce a model that is more stable and effective and to precisely measure the parameters of the PV system ground. The suggested approach can accelerate the algorithm's convergence to accurately evaluate the solar cell ground simulation parameters. The adversarial-based exploratory technique and chaotic drift mechanism have been added to HHO by Chen [13]. In Ref. [14], the moth flame method (MFO) has been illustrated to parameter identification of PV modules by adding a mechanism to improve global convergence and local mining capabilities which results in exceptional performance in the PV SDM and DDM designs. The enhanced Harris hawk algorithm (CCNMHHO) has been utilized by Liu et al. [15] to determine the solar model parameters. To assess the unknown parameters for SDM and DDM, Chen et al. [16] suggested an improved sine cosine technique called ISCA. Using the improved ant-lion optimizer (IALO), Wu et al. [17] suggested a method for parameter evaluation. IALO had successful outcomes with the photovoltaic model.

In order to address the challenge of estimating parameter values for the improved PV modules with SDM and DDM, this research incorporates the QUATRE method with recombination mechanism (RQUATRE) [18]. This addresses the tendency to trap in the nearby extremum and the issue of the slow rate of convergence accuracy of the QUATRE algorithm. The precise constituent PV module parameters have been extracted by combining the Newton Raphson performance approach with Drone Squadron optimization [19]. In order to estimate the unidentified parameters of SDM and DDM, this study in Ref. [20]modified the squirrel search algorithm by minimizing the RMSE. The fractal maps improved the Harris Hawks optimization algorithm in Ref. [21], resulting in the proposal of a new method called FCHHHO and applied on PWP PV module and the RTC France solar cell. Modelling and parameter analysis are carried out with manufacturer datasheet requirements with respect to variations in solar irradiation and ambient temperature. The PV module TRINA TSM-295's ideal parameters are discovered using the suggested method [22]. By employing local escape operators, the study in Ref. [23] enhanced the moth flame algorithm's exploration operator and population diversity. Compared to other methods, this algorithm could produce excellent results, but it needed a large number of function evaluations. By employing quadratic interpolation to speed up convergence and a local search technique to prevent stagnation into local minima, Qaraad et al. in Ref. [24] enhanced the particle swarm optimization. This enhanced version, known as QPSOL, was used to ascertain the unknown parameters of SDM and DDM.

The adaptive variational particle swarm optimizations (PSO) technique was suggested by Merchaoui et al. [25,26] for determining the unidentified parameters of various photovoltaic models and optimizing the best parameters for solar models in different circumstances. Jiao et al. [27] employed generalized opposition-based learning (GOBL) techniques and orthogonal learning (OL) to precisely and effectively assess the solar cells' parameters of PV modules. In order to choose the best design options, Ridha et al. [28] offered an in-depth investigation based on multi-objective optimization and multi-criteria methodologies on stand-alone PV system design. To solve the parameter identification problem for solar cells, Abbassi et al. [29] suggested an improved algorithm based on the Salp swarm algorithm that uses an opposition-based learning approach. Even though NMiH and its variations outperform deterministic methods in terms of solution quality and speed, they have some disadvantages. To start, the technique's convergence speed could be improved. In addition, the method is slightly specialized, and its high performance is only limited to specific types of optimization challenges, which restricts their application areas.

Kepler Optimization Algorithm (KOA) is a novel comprehensive optimization framework that emulates diverse principles based on Kepler's concepts [30]. The KOA is designed to enhance the efficiency of exploration and exploitation within the search space by simulating the dynamic distances of candidate solutions (planets) from the sun at different points in time. In this algorithm, each planet represents a candidate solution concerning the sun, and its position is randomly altered throughout the optimization process. It was effectively applied to solve the economic dispatch with heat optimization in power systems [31]. This study introduces a novel approach by leveraging the SDM and DDM to extract PV components with unknown parameters. The fitness function evaluates the root-mean-square error between the partially estimated model current and experimental values.

The key innovation lies in the development of an advanced Fractional Order Kepler Optimization Algorithm (FO-KOA), integrating Fractional Order (FO) elements with the KOA. FO-KOA introduces FO without relying on intricate derivative solutions, enabling it to efficiently scan for high-quality solutions in the local region. This enhancement significantly improves the local search capability and

solution accuracy of the algorithm. To further balance algorithmic exploration and exploitation, this work incorporates the Local Escaping Approach (LEA) method. This addition boosts population diversity, preventing the algorithm from converging to a local optimum prematurely. The synergistic interplay between FO and LEA empowers FO-KOA with a reasonable split between the exploration and exploitation phases, enhancing its overall performance. To demonstrate the algorithm's efficacy, FO-KOA is tested against more sophisticated algorithms on the SDM, DDM, and PV models. Excellent outcomes are demonstrated by FO-KOA through experimental study.

In brief, the following points are the primary contributions of this paper.

- A revolutionary enhanced FO-KOA is introduced in this paper.
- The proposed FO-KOA has significant advantages and robustness over earlier reported results for both PV modules.
- The algorithm's performance is enhanced by the method using the ideas of FO and LEA, where the FO mechanism enhances the diversity and speed of intelligence, and the LEA finds better high-quality solutions in local areas.
- The SDM and DDM test the algorithm's effectiveness, where there is an excellent match between the simulated and real data.

This document is organized in the following way: The problem definition is presented in Section 2. The proposed new FO-KOA is described entirely in Section 3. Section 4 thoroughly examines the experimental findings and confirms the effectiveness of FO-KOA. The conclusion for this work is discussed in Section 5.

2. Problem formulation of solar PV parameters extraction

The mathematical modeling of PV modules, which are SDM and DDM frameworks, are covered in this section. Beyond that, a discussion of the objective function is employed to resolve the parameter determination issue for the mentioned PV models [32].

2.1. SDM

The SDM can be easily designed as can be observed in Fig. 1 when the solar cell is considered as an internal parallel circuit.

As illustrated in Fig. 1, the symbol (I) represents the circuit's overall output current [33]. The symbol (I_{ph}) stands for photocurrent, I_d for diode current, and the output current (I) can be described as developed in the following equation [34]:

$$I = I_{ph} - I_P - I_{d1} \tag{1}$$

The I_P represents the shunt resistor current can be estimated throughout the following equation [35]:

$$I_P = \frac{I \cdot R_S + V}{R_{Sh}} \tag{2}$$

where R_{Sh} is shunt resistance, R_S is Series resistance and V indicates the output voltage. I_{d1} illustrates the diode current and can be mathematically calculated by Eq. (3) [35].

$$I_{d1} = I_{S1}\left[\exp\left(\frac{I \cdot R_S + V}{\eta_1 \cdot V_{thr}}\right) - 1\right] \tag{3}$$

where η_1 denotes the diode ideal factor, I_{s1} signifies the diode reverse saturation current, and V_{thr} is the junction thermal voltage that can be described in Eq. (4) [36].

$$V_{thr} = \frac{K_B \cdot T}{q_c} \tag{4}$$

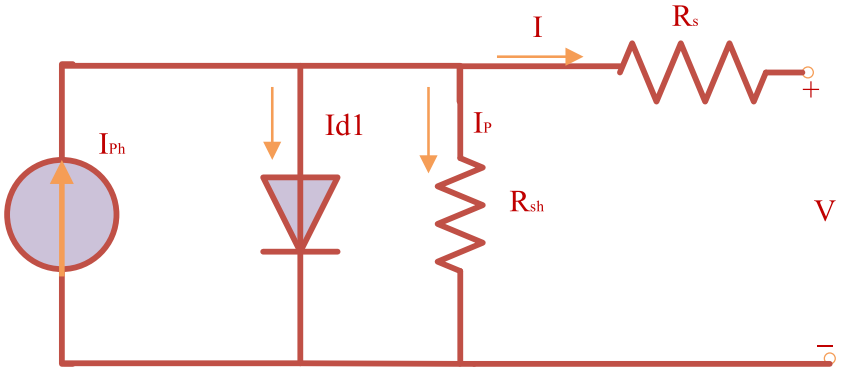

Fig. 1. Representation of SDM circuit.

where K_B denotes Boltzmann's constant (1.380653×10^{-23}J/K), q_c indicates the electron charge of $1.60217646 \times 10^{-19}$C and T indicates temperature in kelvin. In conclusion, the relationship between the output current and other diverse parameters is developed in Eq. (5) by combining the above formulas [37],

$$I = I_{ph} - I_{S1}\left[\exp\left(\frac{I \cdot R_S + V}{\eta_1 \cdot V_{thr}}\right) - 1\right] - \frac{V}{R_{sh}} - \frac{I \cdot R_S}{R_{sh}} \tag{5}$$

It can be observed from Eq. (5) that there are five variables (I_{s1}, I_{ph}, R_{sh}, R_s, and η_1) which require extraction in SDM.

2.2. DDM

The DDM is developed to overcome the loss of compound currents in the SDM. To illustrate, Eq. (25) manifests the calculation of the total current in the equivalent circuit that depicted in Fig. 2 [38].

$$I = I_{ph} - I_{Sh} - I_{d1} - I_{d2} \tag{6}$$

The relationship between the output voltage, output current and other diverse parameters in the DDM is developed in Eq. (7) by combining the above formulas [38],

$$I = I_{ph} - I_{S1}\left[\exp\left(\frac{I \cdot R_S + V}{\eta_1 \cdot V_{thr}}\right) - 1\right] - I_{S2}\left[\exp\left(\frac{I \cdot R_S + V}{\eta_2 \cdot V_{thr}}\right) - 1\right] - \frac{V}{R_{sh}} - \frac{I \cdot R_S}{R_{sh}} \tag{7}$$

where η_1 and η_2 denotes the ideal factor of both diodes, I_{s1} and I_{s2} signify the first and second diode reverse saturation current.

It can be observed from Eq. (7) that there are seven variables (I_{s1}, I_{s2}, I_{ph}, R_{sh}, R_s, η_1 and η_2) which require extraction in DDM.

2.3. PV modules handling

The structure of the photovoltaic module model is more complex, mainly composed of multiple solar cells connected in series or in parallel. The output current illustrated in the equivalent circuit of the PV module model can be described as depicted in Eq. (8) [39].

$$I = N_p\left(\begin{array}{l} I_{ph} - I_{S1}\left[\exp\left(\frac{1}{\eta_1 \cdot N_s \cdot V_{thr}} \times \left(\frac{V}{N_p} + \frac{I \cdot N_s \cdot R_S}{N_p}\right)\right) - 1\right] \\ -I_{S2}\left[\exp\left(\frac{1}{\eta_2 \cdot N_s \cdot V_{thr}} \times \left(\frac{V}{N_p} + \frac{I \cdot N_s \cdot R_S}{N_p}\right)\right) - 1\right] \end{array}\right) - \frac{1}{N_s \cdot N_p \cdot R_{sh}} \times \left(\frac{V}{N_p} + \frac{I \cdot N_s \cdot R_S}{N_p}\right) \tag{8}$$

where N_S and N_P demonstrate the number of series and parallel solar cells, respectively.

2.4. Objective model

The objective of the function can be the difference between the experimental current and the output calculated current in the established model [40]. The goal of this study is to reduce the RMSE, which is characterized as [41]:

$$RMSE = \sqrt{\frac{1}{P \cdot N}\left(\sum_{K=1}^{PN}\left(I_{cal}^{K}\left(V_{exp}^{K}, x\right) - I_{exp}^{K}\right)^2\right)} \tag{9}$$

where V_{exp}^{K} and I_{exp}^{K} refer to the observed voltage and current, whilst PN represents the measured data points number. Furthermore, the symbol (x) reveals the PV identification parameter problem which relates to looking for a solution that minimizes the objective function in the solution space.

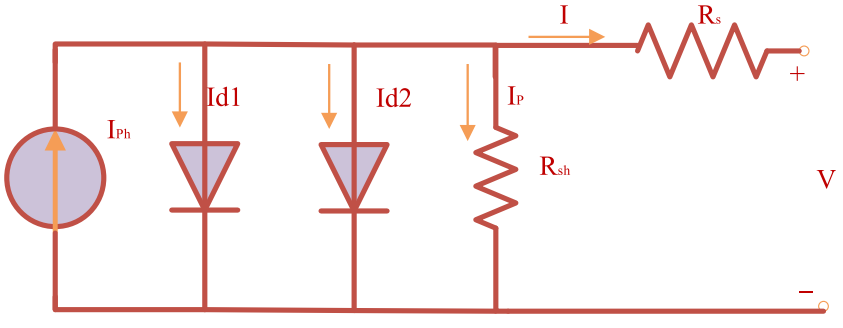

Fig. 2. Representation of the DDM circuit.

3. Proposed FO-KOA for PV parameters extraction

3.1. Standard KOA

Within KOA, every planet performs as a potential solution, whose position is randomly modified in respect to the Sun, which stands for the ideal solution, throughout the optimization process [30,42]. In light of this, the fundamental equation states that, at startup, a number of planets of (N_S) will be allocated at randomly in d dimension, representing the variables that make up the decision of an optimization problem [30]:

$$\overrightarrow{X}_{m,n}(0) = \overrightarrow{X}_{n,l} + q_a \times \left(\overrightarrow{X}_{n,u} - \overrightarrow{X}_{n,l}\right), m = 1 : N_S; n = 1 : d \tag{10}$$

where $X_{m,n}$ represents the solution regarding every planet, and q_a is a randomly generated value having a value spectrum of 0–1. $X_{n,l}$ and $X_{n,u}$ comprise the corresponding lowest and highest limiting values, respectively.

Next, we measure each object's velocity according to its position with regard to the Sun position (X_{SUN}) as follows [42]:

$$Vy_m(t) = \begin{cases} q_b \times \left(\overrightarrow{X}_1 - \overrightarrow{X}_m\right) \times H + \overrightarrow{W}_2 \times F \times \left(1 - R_{m,norm}(t)\right) \times \overrightarrow{q}_c \left(q_d \overrightarrow{X}_{m,u} - \overrightarrow{X}_{m,l}\right) & if\ R_{m,norm}(t) > 0.5 \\ \rho\left(2q_b \overrightarrow{X}_m - \overrightarrow{X}_2\right) - \rho^* \left(\overrightarrow{X}_2 - \overrightarrow{X}_1\right) + \overrightarrow{W}_1 \times F \times \left(1 - R_{m,norm}(t)\right) \times \overrightarrow{q}_c \left(\overrightarrow{X}_{m,u} - \overrightarrow{X}_{m,l}\right) & Else \end{cases} \tag{11}$$

where H, ρ and ρ^* can be defined as follows [42]:

$$H = \left[(m_m + M_{SUN}) \times \mu(t) \times \left|2 \times (R_m(t) + \varepsilon)^{-1} - (a_m(t) + \varepsilon)^{-1}\right|\right]^{0.5} \tag{12}$$

$$\rho = \overrightarrow{W} \times H \times \left(q_e \times \left(1 - q_f\right) + q_f\right) \tag{13}$$

$$\rho^* = \left(1 - \overrightarrow{W}\right) \times H \times \left(q_e \times \left(1 - q_g\right) + q_g\right) \tag{14}$$

Where the mth object position is represented by X_m and its running velocity at time t is described by $Vy_m(t)$; a vector form is indicated by symbol →; W, W_1, W_2 are typically randomly generated numbers chosen from the range of {0,1}; q_a, q_b, q_c, q_d, q_e and q_f have become randomised uniformly distributed numbers between the boundaries of [0,1]; F gets a numerical number that has been selected at random inside band {-1,1}; A small value called ε is employed to prevent divide-by-zero errors; M_{SUN} and m_m, correspondingly, stand in for the masses of X_{SUN} and X_m while X_1 and X_2 have been chosen at random alternatives picked from the total solutions; The general gravitational constant is represented by the symbol $\mu(t)$. At any given time t, the distance between each object X_m and X_{SUN} is represented by $R_m(t)$ while the semimajor axis of the object m's elliptical orbit at that time is indicated by a_m as follows [30]:

$$a_m(t) = q_g \times \sqrt[3]{\frac{(m_m + M_{SUN}) \times OI_m{}^2 \times \mu(t)}{4\pi^2}} \tag{15}$$

where OI_m, that originated via the normal distribution, represents the orbital interval for every mth object. Normalising the Euclidian distance between X_{SUN} and X_m is indicated by the symbol $R_{m,norm}(t)$, which can be explained as follows [30]:

$$R_{m,norm}(t) = \frac{R_m(t) - R_{\min}(t)}{R_{\max}(t) - R_{\min}(t)} \tag{16}$$

During the rotation around the Sun, objects move temporarily nearer to and eventually farther from the Sun. KOA uses two main steps to depict this behaviour: exploration and exploitation. KOA looks for better solutions close to the Sun and also tries out new ideas from places farther away. To do this, it adjusts the positions of objects that are far from the Sun like this [42]:

$$\overrightarrow{X}_m(t+1) = \overrightarrow{X}_m(t) + FL \times \overrightarrow{Vy}_m(t) + (Fg_m(t) + |r|) \times \overrightarrow{W} \times \left(\overrightarrow{X}_{SUN}(t) - \overrightarrow{X}_m(t)\right) \tag{17}$$

where $X_m(t+1)$ denotes the upgraded position of the mth planet at time t+1 and FL represents a flag used to change the searching orientations. The attractive gravitational force between X_{SUN} and X_m is represented by the symbol Fg_m which is estimated by Ref. [42]:

$$Fg_m(t) = e_i \times \mu(t) \times \frac{\left(\overrightarrow{M}_{SUN,norm} \times \overrightarrow{m}_{m,norm}\right)}{\overrightarrow{Rn}_m{}^2 + \varepsilon} + q_h \tag{18}$$

where e_m denotes the eccentricity of each orbiting planet (m) while $M_{SUN,\ norm}$ and $m_{m,norm}$ denote the normalised quantities of M_{SUN} and m_m, corresponding to the masses of X_{SUN} and X_m, accordingly as follows [42]:

$$\overrightarrow{M}_{SUN,norm} = q_b \times (fitness_{SUN}(t) - worst(t)) \Big/ \left(\sum_{k=1}^{N_S} (fitness_k(t) - worst(t)) \right) \tag{19}$$

$$\overrightarrow{m}_{m,norm} = (fitness_m(t) - worst(t)) \Big/ \left(\sum_{k=1}^{N_S} (fitness_k(t) - worst(t)) \right) \tag{20}$$

Additionally, Rn_m denotes the normalised value of R_m, which essentially represents the Euclidian distance [30]:

$$Rn_m(t) = \sqrt{\sum_{m=1}^{d} (X_{SUN}(t) - X_m(t))^2} \tag{21}$$

where the choice for a solution featuring the greatest fitness grade is shown by *worst(t)*, q_b represents a randomly selected integer between 0 and 1 that is used to separate the masses of several planets. The function $\mu(t)$ is given by the following description. Its function governs the precision of searches by declining exponentially over time (t) [30].

$$\mu(t) = \mu_o \times e^{-\alpha \frac{t}{T_{\max}}} \tag{22}$$

where α stands for a constant, μ_o for the initial value, t for the current iteration, and $T_{\max}$ for the maximum number of iterations.

KOA will focus on enhancing the exploitation where planets come close to the Sun, and it will enhance the exploration driver whenever the Sun gets farther away. The mathematical expression of this concept can be applied as follows to further improve both operators [30]:

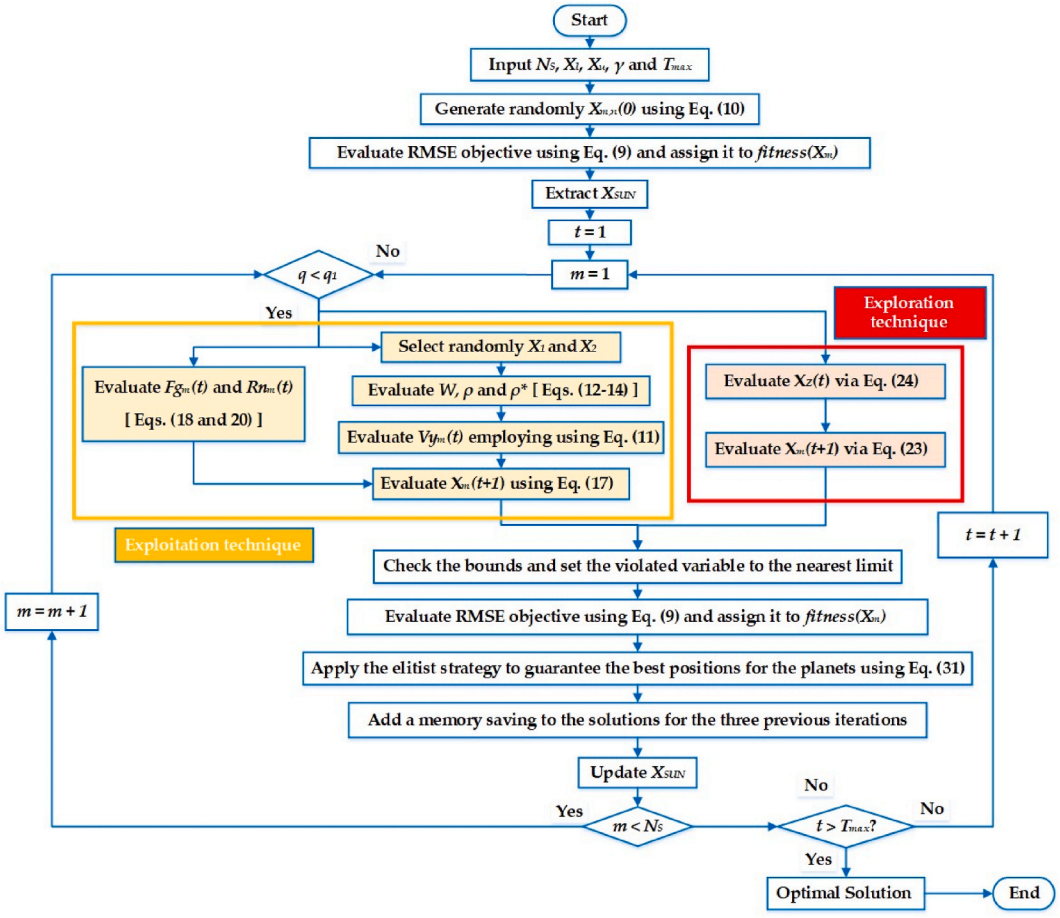

(a)

Fig. 3(a). Standard KOA Flowchart.

$$\vec{X}_m(t+1) = \vec{W}_1 \times \vec{X}_m(t) + \left(\vec{X}_Z(t) + \frac{1}{e^{\left(q \times \left(1 + \left(-2 - \frac{t}{T_{\max}}\right) \times q_y\right)\right)}} \times \left(\vec{X}_Z(t) - \vec{X}_2(t)\right) \right) \times \left(1 - \vec{W}_1\right) \tag{23}$$

$$\vec{X}_Z(t) = \frac{\vec{X}_m(t) + \vec{X}_{SUN} + \vec{X}_1(t)}{3} \tag{24}$$

where q is an unknown number generated by the normal distribution.

Using an elitist method, the final phase, elitism, guarantees the best positions for the planets and the Sun as follows [42]:

$$\vec{X}_{m_{New}}(t+1) = \begin{cases} \vec{X}_m(t+1) & \text{if } finess\left(\vec{X}_m(t+1)\right) \le finess\left(\vec{X}_m(t)\right) \\ \vec{X}_m(t) & Else \end{cases} \tag{25}$$

The main steps of the typical KOA are shown in Fig. 3(a).

3.2. Proposed FO-KOA

The previously mentioned KOA typically uses two different updating algorithms to estimate the planet locations which are exploration approach via Equation (24) and exploitation technique via Equation (17), as illustrated in Fig. 3(a). A contrast involving two arbitrary numbers {q, q_1} is used to execute the exchange between both techniques. The transferring process roughly corresponds to an equal method. Consequently, the exploitation approach will activate using roughly half of the answers for each iteration starting at the beginning of the iteration trip. To boost its search efficiency, this section presents a ground-breaking augmented Fractional Order KOA (FO-KOA). The primarily engaged change employs a fractional order element to achieve effective information and past expertise sharing amongst the participants with the goal of avoiding premature converging. Added to that, the Local Escaping Approach (LEA) [42] has been incorporated to boost the search procedure by evading local optimization.

Every object's variation between its entirely created and present locations has the potential to be numerically approximated in the manner shown below for the purpose to include the fractional order element [43]:

$$\vec{X}_m(t+1) = \vec{X}_m(t) + \underbrace{\left[\left|\sum_{k=1}^{L} (-1)^k \frac{\Gamma(\zeta+1) \times \vec{X}_m(t-kT)}{\Gamma(k+1) \times \Gamma(\zeta-k+1)}\right|\right]}_{\underline{Fractional\ order\ element}} \text{ if } t > 3 \tag{26}$$

where T is the sample interval, and ζ is generally a real number, called the fractional-order.

The stored data and hereditary parts of the motivated response have been described in the process to expedite the exploration strategy based on the framework that is suggested. Each of the possible solutions employed memories when relocating an object in accordance with the combined strategy, and the revised positions of each object may be calculated and simplified as follows [43]:

$$\overrightarrow{Ob}_i(t+1) = \overrightarrow{Ob}_i(t) + \underbrace{[FOE_1 \times Ob_i(t) + FOE_2 \times Ob_i(t-1) + FOE_3 \times Ob_i(t-2) FOE_4 \times Ob_i(t-3)]}_{\underline{Fractional\ order\ element}} if\ t > 3 \tag{27}$$

$$FOE_1 = \frac{1}{1!}\zeta \tag{28}$$

$$FOE_2 = \frac{1}{2!}\zeta(1-\zeta) \tag{29}$$

$$FOE_3 = \frac{1}{3!}\zeta(1-\zeta)(2-\zeta) \tag{30}$$

$$FOE_4 = \frac{1}{4!}\zeta(1-\zeta)(2-\zeta)(3-\zeta) \tag{31}$$

As mentioned in Eq. (27), this approach does not provide any additional benefit if the current iteration exceeds three. Reliance on past memories is the root of this syndrome.

Additionally, a LEA is being added to improve the procedure of searching by avoiding local optimization, which could change some planets' locations during every iteration. To do so, Eq, (32) is proposed as follows:

$$\vec{X}_m(t+1) = \begin{cases} \vec{X}_m(t) + \phi_1\left(\beta_1 \vec{X}_{SUN} - \beta_2 \vec{X}_1\right) + \frac{1}{2} \times \beta_2 \phi_2 \sigma_1 \times \left(\vec{X}_2 - \vec{X}_3\right) & \text{if } q_o < 0.5 \\ & \text{if } q_p < Q_w \\ \vec{X}_{SUN} + \phi_1\left(\beta_1 \vec{X}_{SUN} - \beta_2 \vec{X}_1\right) + \frac{1}{2} \times \beta_2 \phi_2 \sigma_1 \times \left(\vec{X}_2 - \vec{X}_3\right) & Else \end{cases} \tag{32}$$

where Q_w is a probabilistic variable that controls LEA stimulating. q_o and q_p represent arbitrarily quantities in the interval [0, 1]; ϕ_1 and ϕ_2 are randomized numbers in the range [-1; 1]; and X_1, X_2, and X_3 represent various randomly chosen solutions. Additionally, σ_1, β_1, and β_2 are randomised numbers generated adaptively, similar to Ref. [42]. The main steps of the proposed FO-KOA are shown in Fig. 3 (b).

4. Simulation results and discussions

This part studies the KC200GT, the Ultra 85-P PV panel, SP70 and RTC France cell using the proposed FO-KOA and KOA techniques. The first module is Kyocera type KC200GT (multi-crystalline), where 54 series-connected cells have currents of 8.21 A and 7.61 A at SC and MP, respectively, and voltages of 32.90 V and 26.30 V at OC and MP, respectively. This module has a 200 W MP rating. Fifteen sets of related I and V values for the KC200GT make up the actual dataset points. The second module is the commercialized module Ultra 85-P, where this panel, which consists of 36 monocrystal-line PV cells connected in series, has a maximum output of 85 W at STC with a tolerance of 5 %. This module has an efficiency of 13.4 % and a fill factor of 70.3 %. A 20 A series fuse is used to protect this panel, which is 120.0 cm in length, 52.70 cm in width, and 3.40 cm in depth. It weighs 7.5 kg. The complete datasheet for this module is accessible at [44]. The third module is SP 70 (monocrystalline), with a power rating of 70 W. This unit has 36 cells connected in series to create a total current of 4.70 A SC, and 4.24 A at MP, with voltages of 21.4 V at OC and 16.5 V at MP. The fourth testing study is the well-known solar cell - RTC France solar cell.

The selection of the Kyocera KC200GT, Ultra 85-P, and SP70 PV modules in this study is driven by specific considerations. At first, they are widely utilized in solar energy applications, making them a representative choice for analysis, as they are highly relevant and applicable to real-world scenarios. Second, they serve as a benchmark for evaluating the optimization algorithms against other state-of-the-art optimization algorithms. This benchmarking approach enables a thorough assessment of the proposed algorithm's efficacy in

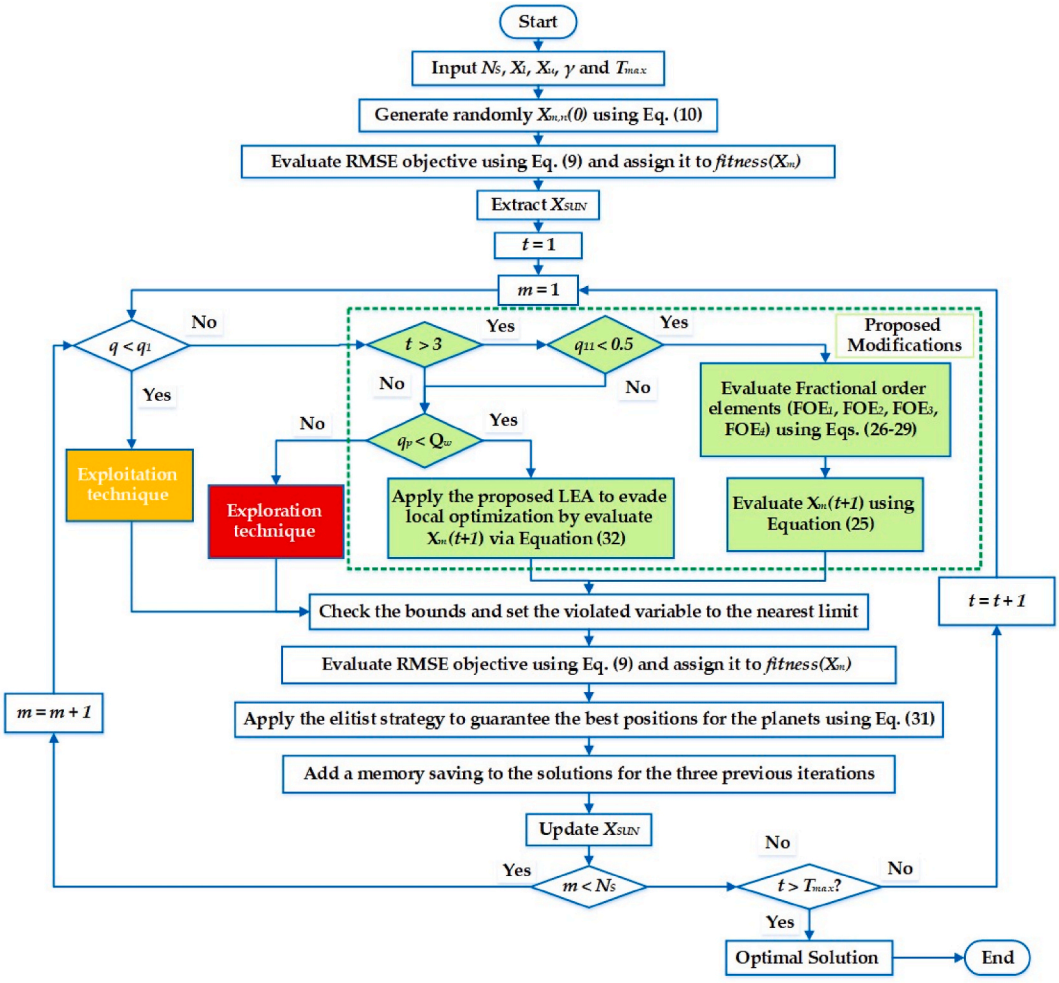

(b)

Fig. 3 (b). Proposed FO-KOA Flowchart.

comparison to existing methods [45–54]. Third, they are distinguished with diversity in technology offering diversity in the characteristics and parameters of the photovoltaic systems under investigation.

For the four solar systems under consideration, Table 1 shows the lower and upper limits of the parameters. Eight case studies are elaborated in this study to show the ability of the proposed FO-KOA to obtain the PV cell parameters.

4.1. Application for the KC 200 PV module

4.1.1. Case 1: the SDM (KC 200 PV module)

In this case, the proposed FO-KOA and the KOA are used to extract the SDM parameters of the Kyocera KC200GT PV Module. Table 2 displays the five unidentified SDM parameters for which each algorithm's optimal results were attained during the experiment. The findings demonstrate the superior competitiveness of the proposed FO-KOA over the KOA and comparative algorithms. Specifically, the FO-KOA earned the best RMSE value (7.5359 E−04) while the conventional KOA achieved an RMSE of 1.3513025 E−2. This improvement amounts to 94.43 % of the changes in the FO-KOA that were suggested for this case. Furthermore, the table exhibits the PV extracted electrical parameters using the reported optimization optimizers which are HEAP Optimizer [46], multi-verse optimizer (MVO) [48], an Enhanced MPA (EMPA) [46] neighborhood scheme-based Laplacian MBA (NLBMA) [49], Forensic-Based Investigation Optimizer (FBI) [50], Hybrid Firefly and Pattern Search (HFAPS) [51], particle swarm optimization (PSO) [52], Barnacles Mating Optimizer (BMA) [53], Equilibrium Optimizer (EO) [46], Lightning Attachment Procedure Optimization (LAPO) [54], Classified perturbation mutation PSO (CPMPSO) [55], Jellyfish Search (JFS) Optimizer [46], Ant Lion Optimizer (ALO) [56], Growth optimizer (GO) [57], flexible PSO (FPSO) [2], Marine Predator (MPA) Algorithm [46], hybrid PSO–GWO algorithm (PSOGWO) [58], and Enriched Harris Hawks optimization (EHHO) [13]. Besides, this table signifies the estimated parameters of (FO-KOA and KOA) which are (8.21587363 A and 8.177105972 A), (0.00481849 Ω and 0.00467622 Ω), (6.41929739 Ω, 41.84111455 Ω), (2.7002E-02 μA and 5.16881E-02 μA), and (1.21470625 and 1.256166834), for the photo-current, series, shunt resistances, saturation current for d1, and ideality factor for d1, respectively. Moreover, this table expresses the electrical parameters obtained using other inspiring optimizers.

In Fig. 4, the convergence curves are displayed. As illustrated in this figure, the FO-KOA converged quite quickly in the first 80 iterations which shows the great ability of FO-KOA to converge. Moreover, Fig. 5 illustrates the KOA and FO-KOA boxplot of the thirty obtained RMSE objectives for Case 1. As shown, the proposed FO-KOA exhibits notable advancements in all measured aspects. Specifically, in terms of the mean value, the FO-KOA achieves a reduction from 0.018033335 to 0.006127644, marking a substantial 66.02 % enhancement. Similarly, the worst value sees a significant improvement, decreasing from 0.026026056 with KOA to 0.009882305 with FO-KOA, representing a 62.03 % reduction in error. The FO-KOA also excels in maximizing performance, with the standard deviation dropping from 0.003427786 to 0.002178863, showcasing a 36.44 % decrease in error. It can be observed that the RMSE of FO-KOA is between [7.5359 E−04 to 1.1 E−02], whilst the RMSE of KOA is between [1.5 E−02 to 2.6 E−02]. As a result, the proposed FO-KOA obtained the best value, showing that FO-KOA has more stability than KOA as well as higher precision and reliability in its comparison process for finding SDM parameters. The FO-KOA's identification of the SDM's correctness can be trusted.

4.1.2. Case 2: the DDM (KC 200 PV module)

In this case, the proposed FO-KOA and the KOA are used to extract the DDM parameters of the Kyocera KC200GT PV Module. Table 3 displays the seven unidentified DDM parameters for which each algorithm's optimal results were attained during the experiment. The results reveal that the proposed FO-KOA has excellent competitiveness in contrast to the KOA and the comparison algorithms, where the proposed FO-KOA obtained the best RMSE value (3.53 E−04) while the conventional KOA achieved an RMSE of 1.0554 E−2. This improvement amounts to 96.65 % of the changes in the FO-KOA that were suggested for Case 2. Furthermore, the table exhibits the PV extracted electrical parameters using the reported optimization optimizers which are HEAP Optimizer [46], LAPO [54], an EMPA [46], NLBMA [49], FBI [50], PSO [52], BMA [53], EO [46], JFS [46], Gorilla Troop Optimizer (GTO) [46], GO [57], MPA [46], and PSOGWO [58].

Besides, this table signifies the estimated parameters of (FO-KOA and KOA) which are (8.216025 A and 8.205861 A), (0.00487 Ω and 0.004642 Ω), (6.500292 Ω, 8.576525 Ω), (5.49E-02 μA and 4.56E-02 μA), (4.16E-03 μA and 1.67E-01 μA), (1.328864 and 1.248949), and (1.133816 and 1.768874), for the photo-current, series, shunt resistances, saturation current for (d1 and d2) and ideality factor for (d1 and d2), respectively. Moreover, this table expresses the electrical parameters obtained using other inspiring optimizers.

In Fig. 6, the convergence curves are displayed. As illustrated in this figure, the FO-KOA converged quite quickly in the first 75 iterations which shows the great ability of FO-KOA to converge. Additionally, Fig. 7 illustrates the KOA and FO-KOA boxplot of the

Table 1
The boundaries range for investigating solar cell parameters.

Parameter	KC200GT		Ultra 85-P PV panel		SP70		RTC France	
	Lower	Upper	Lower	Upper	Lower	Upper	Lower	Upper
I_{ph} (A)	0	10	0.00	10.00	0	55	0.00	10.00
I_{S1} and I_{S2} (μA)	0	10	0.00	10.00	0	1	0.00	10.00
η_1 and η_2 per cell	1	2	1.00	2.00	1	2	1.00	2.00
R_S (Ω)	0	0.5	0.00	2.00	0	0.5	0.00	2.00
R_{Sh} (Ω)	0	100	0.00	100.00	0	100	0.00	100.00

Table 2
Extracted PV cell Parameters based on FO-KOA versus KOA and other reported techniques applied on of KC200GT for Case 1.

Algorithm	I_{ph}(A)	I_{S1}(μA)	η_1	R_{Sh}(Ω)	R_s(Ω)	*RMSE*
FO-KOA	8.21587363	2.7002E-02	1.21470625	6.41929739	0.00481849	7.54E-04
KOA	8.177105972	5.16881E-02	1.256166834	41.84111455	0.00467622	1.35E-02
MPA [46]	8.184927	7.94459E-02	1.285180059	92.14823504	0.004537611	1.49E-02
FBI [50]	8.217030039	2.72156E-02	1.215208065	6.235899986	0.004814219	9.88E-04
EO [46]	8.209153	2.85E-02	1.218068	7.714703	0.004815	2.89E-03
JFS [46]	8.193182	4.72E-02	1.250052	14.97462	0.004679	9.48E-03
GO [57]	8.192967	4.31808 E−02	1.244346	15.103921	0.004710	8.52E-03
CPMPSO [55]	8.21689146	0.00224195	1.07641028	763.535149	0.34381405	1.54E-03
EHHO [13]	8.2224	0.000001	80.6915	1806.0252	0.1835	5.95E-02
PSO [52]	8.2027	2.8852	1.6052	33.8855	0.0019	1.02E-01
FPSO [2]	8.2186	0.001436	56.9854	130.2813	0.2409	2.82E-02
HEAP [46]	8.200974	4.49E-02	1.246924	11.87468	0.004696	7.43E-03
LAPO [54]	8.2155	8.1491	1.7258	5.0000	0.001	1.38E-01
HFAPS [51]	8.1992	0.154161	74.5795	1448.2590	0.2396	4.99E-02
PSOGWO [58]	8.2132	9.6768	1.7463	38.8968	0.0011	1.27E-01
MVO [48]	8.2527	0.063908	69.2388	134.4813	0.1341	8.38E-02
NLBMA [49]	8.1467	0.0022	1.0839	5.0000	0.0045	3.36E-02
BMA [53]	8.1950	3.1015	1.6130	100.0000	0.0019	1.02E-01
EMPA [46]	8.21195	3.59E-02	1.232551	7.560713	0.004742	3.85E-03

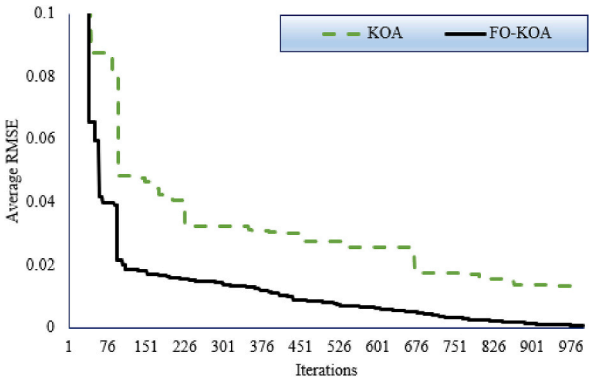

Fig. 4. KOA and FO-KOA Converging curves for Case 1.

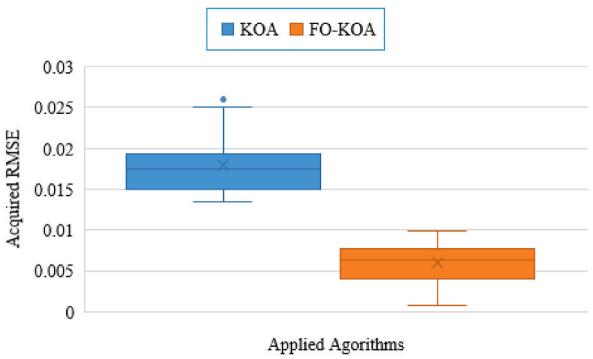

Fig. 5. KOA and FO-KOA Boxplot of the thirty acquired RMSE objective for Case 1.

thirty obtained RMSE objectives for Case 2. This comparison reveals substantial improvements in tilizing the proposed FO-KOA in various performance metrics. Specifically, the minimum value attained by the FO-KOA significantly decreases from 0.010554145 with KOA to 0.000352854, indicating an impressive 96.66 % enhancement. Furthermore, the mean value experiences a notable reduction, declining from 0.023922447 with KOA to 0.006691447 with FO-KOA, showcasing a substantial 72.03 % improvement. In terms of maximizing performance, the FO-KOA also demonstrates superiority, with the maximum value decreasing from 0.03834529 to 0.019134773, resulting in a 50.10 % reduction in error. Moreover, the standard deviation sees a considerable decrease from 0.006767701 with KOA to 0.004469515 with FO-KOA, indicating a 33.96 % improvement. These results underscore the significant

Table 3
Extracted PV cell Parameters based on FO-KOA versus KOA and other reported techniques applied on KC200GT for Case 2.

Algorithm	I_{ph}(A)	R_s(Ω)	R_{Sh}(Ω)	I_{S1}(μA)	I_{S2}(μA)	η_1	η_2	*RMSE*
FO-KOA	8.216025	0.00487	6.500292	5.49E-02	4.16E-03	1.328864	1.133816	3.53 E−04
KOA	8.205861	0.004642	8.576525	4.56E-02	1.67E-01	1.248949	1.768874	1.0554E-02
GTO [46]	8.216007	0.00485	6.517429	2.07E-02	7.49E-01	1.199424	1.966626	3.736E-04
LAPO [54]	8.2000	0.0015	96.4369	2.5285	0.1000	1.6147	1.9852	1.1696E− 1
EMPA [46]	8.030514	0.033369	27.27485	4.25E-02	3.48	1.380775	1.351166	2.425 E−03
GO [57]	8.193643	0.004689	16.378287	6.01244 E−02	4.57891E-02	1.832451	1.248347	9.049475 E−03
MPA [46]	8.030354	0.032728	30.53537	2.62	4.25	1.067697	1.372776	2.505 E−03
PSO [52]	8.2000	0.0010	49.0582	0.0010	0.1000	1.2801	1.7522	1.2970E− 1
BMA [53]	8.2000	0.0012	100.0000	0.0010	9.4407	1.3396	1.7449	1.2492E− 1
JFS [46]	8.030293	0.033339	28.17502	2.35	1.19	1.356141	1.346628	2.426 E−03
HEAP [46]	8.030409	0.033326	28.33547	3.56	0	1.353583	1.354422	2.428 E−03
NLBMA [49]	8.2000	0.0010	49.0582	0.0010	0.1000	1.2801	1.7522	3.3043E− 2
PSOGWO [58]	8.2000	0.0013	97.9874	0.0010	8.1150	1.3240	1.7260	1.2178E− 1
EO [46]	8.03054	0.033375	27.17874	1.04	2.44	1.351035	1.35097	2.425 E−03
FBI [50]	8.030533	0.033336	27.29641	0.0771	3.44	1.335552	1.352567	2.425 E−03

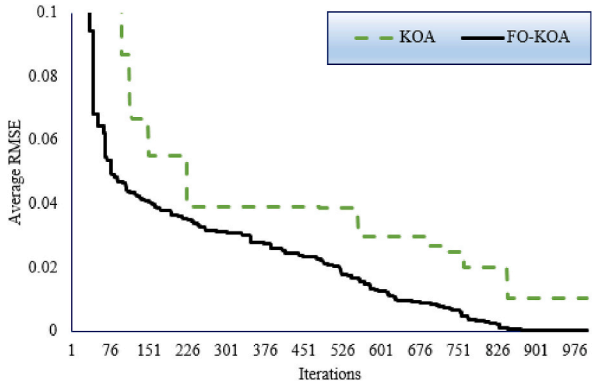

Fig. 6. KOA and FO-KOA Converging curves for Case 2.

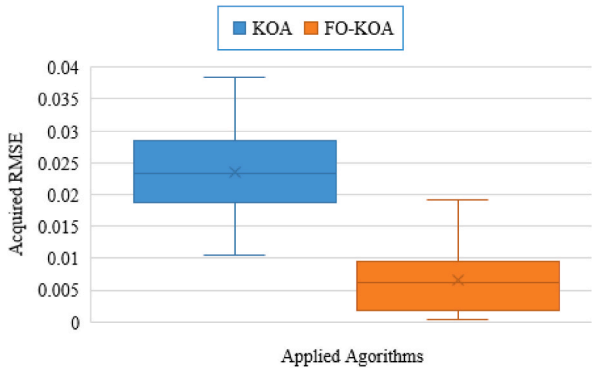

Fig. 7. KOA and FO-KOA boxplot of the thirty obtained RMSE objective for Case 2.

advancements achieved by the FO-KOA over the conventional KOA.

While it's acknowledged that algorithms like Artificial Hummingbird Algorithm (AHA) [45] has shown promise in solving PV modules extraction problem. In this paper, AHA sowed better performance compared to Teaching learning studying-based optimizer (TLSBO), African vultures optimizer (AVO) and Tuna swarm optimizer (TSO). Through the comparison between the proposed FO-KOA and the reported results of [45], the proposed FO-KOA demonstrates better performance. Specifically, the mean value experiences a notable reduction of 30.87 % compared to the AHA, declining from 9.68E-03 to 0.006691 with FO-KOA. Also, the proposed FO-KOA showcases a substantial 57.62 % improvement compared to the TLSBO which acquired a mean value of 1.58E-02. In comparison to the AVO, the FO-KOA also demonstrates superiority resulting in a 79.17 % reduction in RMSE. Moreover, the proposed FO-KOA achieves a considerable decrease from 4.29E-02 with TSO to 0.006691with FO-KOA, indicating an 84.4 % improvement.

Fig. 8 displays the I–V curve and P–V curve of the DDM of the KC 200 PV Module that are produced from the best FO-KOA simulation settings and the actual measurement data, respectively, in order to further represent the experimental results. This figure illustrates the higher precision and reliability of the FO-KOA to obtain the current and power with different voltage levels.

Furthermore, Table 4 highlights the improvement percentage of the proposed FO-KOA in comparison with the reported techniques. The results presented in Table 4 demonstrate the superior performance of the proposed FO-KOA compared to several reported optimization techniques for extracting PV cell parameters, particularly for the KC200GT module in Cases 1 and 2. For case 1, while KOA performs well with an RMSE of 1.35E-02, FO-KOA outperforms it by 94.42 %, indicating substantial enhancement. Additionally, the proposed FO-KOA consistently outperforms other algorithms by substantial improvement percentages, ranging from 23.73 % to 99.26 %, demonstrating its robustness across various optimization methods. For case 2, KOA achieves RMSE of 1.06E-02, and FO-KOA outperforms it by 96.60 %, highlighting its consistent superiority. Also, FO-KOA exhibits higher improvement percentages over the others, ranging from 5.51 % to 99.73 %, emphasizing its effectiveness and reliability.

4.2. Application for the Ultra Power 85 PV module

4.2.1. Case 3: application for the SDM

In this case, the proposed FO-KOA and the KOA are used to extract the SDM parameters of the Kyocera KC200GT PV Module. Table 5 displays the five unidentified SDM parameters for which each algorithm's optimal results were attained during the experiment. Furthermore, the table exhibits the PV extracted electrical parameters using the recently developed optimizers which are the Dwarf mogoose optimization (DMO) [59–62] neural network optimization algorithm (NNA) [63], the zebra optimization algorithm (ZOA) [64] and the Mantis search Algorithm (MSA) [65]. It can be illustrated from the table that the proposed FO-KOA obtained the best RMSE value (0.00356316), while KOA obtained the best RMSE value (0.004583598). This improvement amounts to 22.26 % of the changes in the FO-KOA that were suggested for Case 3. The results reveal that the proposed FO-KOA has excellent competitiveness in contrast to the KOA and the comparison algorithms. Also, Fig. 9 depicts the convergence curves for the proposed FO-KOA, KOA, DMO, NNA, ZOA, and MSA. As shown, the proposed FO-KOA derives better performance compared to ZOA, DMO, MSA, and NNA as well.

Moreover, Fig. 10 illustrates KOA, FO-KOA, DMO, NNA, ZOA, and MSA boxplot of the thirty obtained RMSE objectives for Case 3. It presents the performance metrics of various optimization algorithms, including MSA, DMO, NNA, ZOA, KOA, and the proposed FO-KOA. Across these algorithms, notable differences in their minimum, mean, maximum, and standard deviation values are observed.

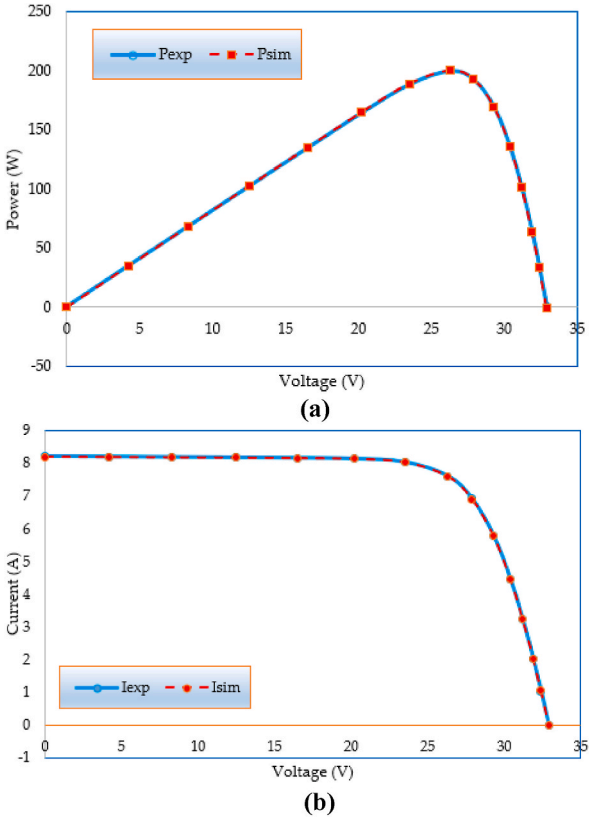

Fig. 8. (a)P–V curve based on FO-KOA for Case 2
Fig. 8(b). I–V curve based on FO-KOA for Case 2.

Table 4
Percentage of improvement of the FO-KOA compared to other methods for different PV cell parameters of KC200GT for Cases 1 and 2.

Case 1			Case 2		
Algorithm	*RMSE*	*Improvement (%)*	Algorithm	*RMSE*	*Improvement (%)*
FO-KOA	7.54E-04	–	FO-KOA	3.53E-04	–
KOA	1.35E-02	94.42 %	KOA	1.06E-02	96.66 %
MPA [46]	1.49E-02	94.93 %	GTO [46]	3.74E-04	5.51 %
FBI [50]	9.88E-04	23.73 %	LAPO [54]	1.17E-01	99.70 %
EO [46]	2.89E-03	73.91 %	EMPA [46]	2.43E-03	85.44 %
JFS [46]	9.48E-03	92.05 %	GO [57]	9.05E-03	96.10 %
GO [57]	8.52E-03	91.15 %	MPA [46]	2.51E-03	85.91 %
CPMPSO [55]	1.54E-03	51.03 %	PSO [52]	1.30E-01	99.73 %
EHHO [13]	5.95E-02	98.73 %	BMA [53]	1.25E-01	99.72 %
PSO [52]	1.02E-01	99.26 %	JFS [46]	2.43E-03	85.45 %
FPSO [2]	2.82E-02	97.33 %	HEAP [46]	2.43E-03	85.46 %
HEAP [46]	7.43E-03	89.85 %	NLBMA [49]	3.30E-02	98.93 %
LAPO [54]	1.38E-01	99.45 %	PSOGWO [58]	1.22E-01	99.71 %
HFAPS [51]	4.99E-02	98.49 %	EO [46]	2.43E-03	85.44 %
PSOGWO [58]	1.27E-01	99.41 %	FBI [50]	2.43E-03	85.44 %
MVO [48]	8.38E-02	99.10 %			
NLBMA [49]	3.36E-02	97.76 %			
BMA [53]	1.02E-01	99.26 %			
EMPA [46]	3.85E-03	80.41 %			

Table 5
Extracted Parameters based on FO-KOA, KOA, and recently developed techniques for Case 3.

Item	ZOA	DMO	MSA	NNA	KOA	FO-KOA
I_{ph}(A)	5.180799436	5.209587967	5.22749264	5.22741374	5.220997273	5.22751202
R_s (Ω)	0.010118476	0.010647702	0.01107435	0.01107121	0.010937032	0.01107487
R_{sh} (Ω)	23.47359277	4.952758368	3.76444247	3.77066218	3.997888277	3.76304503
I_{S1} (A)	3.1682E-05	1.64942E-05	1.0112E-05	1.015E-05	1.13919E-05	1.0106E-05
η_1	1.711091626	1.624721679	1.56462094	1.56506249	1.578812397	1.56455772
RMSE	0.013722439	0.008172571	0.0035632	0.00356342	0.004583598	0.00356316

For instance, the minimum error achieved by the FO-KOA stands out as the lowest among all algorithms, with a value of 0.003563162. Similarly, the mean error for FO-KOA is significantly lower compared to other algorithms, indicating its consistent performance in generating accurate solutions. Moreover, the maximum error for FO-KOA is notably lower than that of the other algorithms, suggesting its effectiveness in avoiding large deviations from optimal solutions. Additionally, the standard deviation of FO-KOA is remarkably lower than that of KOA, underscoring its improved consistency and reliability in producing solutions. It can be observed from this figure that the range of RMSE of FO-KOA is very small compared with KOA, DMO, NNA, ZOA, and MSA. As a result, the FO-KOA's identification of the SDM's correctness can be trusted. Based on the average obtained RMSE, the proposed FO-KOA shows improvement with 3.762 %, 63.473 %, 68.373 %, 84.846 %, and 45.205 %, respectively compared to MSA, DMO, NNA, ZOA, and KOA.

4.2.2. Case 4: application for the DDM

In this case, the proposed FO-KOA and the KOA are used to extract the DDM parameters of the Kyocera KC200GT PV Module. Table 6 displays the seven unidentified DDM parameters for which each algorithm's optimal results were attained during the experiment. Furthermore, the table exhibits the PV-extracted electrical parameters using the recently developed optimizers which are

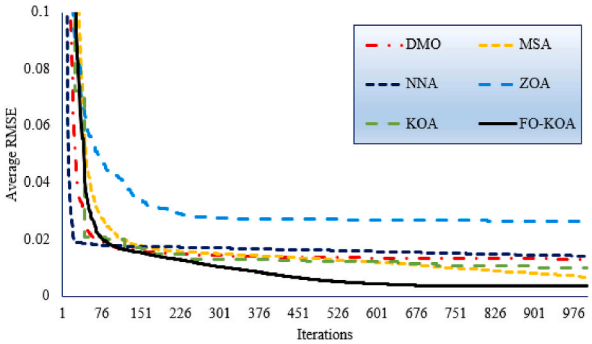

Fig. 9. KOA, FO-KOA, ZOA, DMO, NNA, and MSA Converging curves for Case 3.

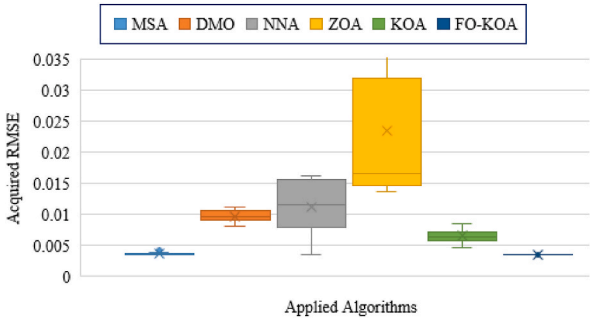

Fig. 10. KOA, FO-KOA, ZOA, DMO, NNA, and MSA boxplot of the thirty obtained RMSE objective for Case 3.

DMO [59,60], NNA [63], ZOA [54], and MSA. It can be noticed that the proposed FO-KOA obtained the best RMSE value (0.00341), while KOA obtained the best RMSE value (0.009964). The results reveal that the proposed FO-KOA has excellent competitiveness in contrast to the KOA and the comparison algorithms. Otherwise, Fig. 11 illustrates the convergence curves for the proposed FO-KOA, KOA, DMO, NNA, ZOA, and MSA. The proposed FO-KOA obtained the best value at 450 iterations, showing that FO-KOA has more stability than KOA as well as higher precision and reliability in its comparison process for finding SDM parameters. As shown, the proposed FO-KOA derives better performance compared to ZOA, DMO, MSA, and NNA as well.

Moreover, Fig. 12 illustrates the KOA, FO-KOA, DMO, NNA, ZOA, and MSA boxplot of the thirty obtained RMSE objectives for Case 4. Notably, the FO-KOA achieves the lowest minimum error of 0.003409882, indicating its capability to produce highly accurate solutions. Moreover, the mean error for FO-KOA (0.003519205) is comparatively lower than other algorithms, suggesting its consistency in generating solutions closer to the optimal solution. Additionally, the maximum error for FO-KOA (0.003567312) remains notably lower, signifying its effectiveness in avoiding large deviations from optimal solutions. Furthermore, the standard deviation of FO-KOA (4.6368E-05) is considerably smaller compared to other algorithms, indicating its stability and reliability in producing consistent results. As a result, the FO-KOA's identification of the DDM's correctness can be trusted. Based on the average obtained RMSE, the proposed FO-KOA shows improvement with 46.062 %, 72.764 %, 74.956 %, 86.487 %, and 74.758 %, respectively compared to MSA, DMO, NNA, ZOA, and KOA.

Fig. 13 displays the I–V curve and P–V curve of the DDM of the KC 200 PV Module that are produced from the best FO-KOA simulation settings and the actual measurement data, respectively, in order to further represent the experimental results. This figure illustrates the higher precision and reliability of the FO-KOA to obtain the current and power with different voltage levels.

4.3. Application for the SP 70 PV module

4.3.1. Case 5: application for the SDM

In this case, the proposed FO-KOA and the KOA are used to extract the SDM parameters of the SP 70 PV Module. Table 7 displays the five unidentified parameters for which each algorithm's optimal results were attained during the experiment. It can be noticed that the proposed FO-KOA obtained the best RMSE value (0.00049369), while KOA obtained the best RMSE value (0.008798587). This improvement amounts to 94.38 % of the changes in the FO-KOA that were suggested for Case 5. The results reveal that the proposed FO-KOA has excellent competitiveness in contrast to the KOA.

In Fig. 14, the convergence curves are displayed for the proposed FO-KOA, in comparison with KOA. The proposed FO-KOA obtained the best value at 450 iterations, showing that FO-KOA has more stability than KOA as well as higher precision and reliability in its comparison process for finding SDM parameters.

Moreover, Fig. 15 illustrates the KOA and FO-KOA boxplot of the thirty obtained RMSE objectives for Case 5. It can be observed from this figure that the RMSE of FO-KOA is between [4.9369 E −04 to 5 E−03], whilst the RMSE of KOA is between [1 E −02 to 1.5 E−02]. As a result, the FO-KOA's identification of the SDM's correctness can be trusted.

Table 6
Extracted Parameters based on KOA and FO-KOA for Case 4.

Item	ZOA	NNA	DMO	MSA	KOA	FO-KOA
I_{ph}(A)	5.178701	5.217579	5.192576	5.225245	5.190564	5.224607
R_s (Ω)	0.010246	0.010967	0.010186	0.011028	0.010573	0.011353
R_{Sh} (Ω)	23.72715	4.809504	10.09142	3.894603	8.135853	4.170814
I_{S1} (A)	1.87E-05	2.88E-05	4.17E-06	1.85E-07	8.26E-06	3.68E-05
η_1	1.716773	2	1.602714	1.995047	1.87516	1.988842
I_{S2} (A)	1.01E-05	5.64E-06	2.46E-05	1.06E-05	1.44E-05	2.28E-06
η_2	1.669564	1.517106	1.726106	1.570357	1.61898	1.42941
RMSE	0.013473	0.004673	0.011392	0.003621	0.009964	0.00341

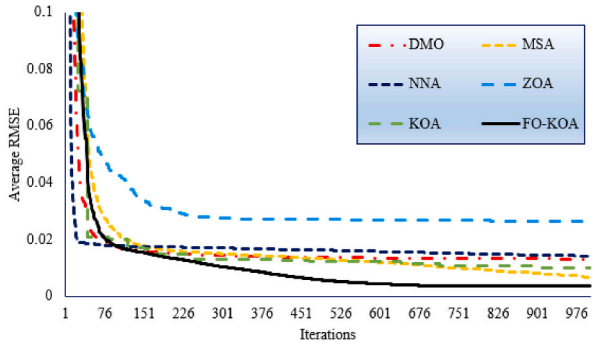

Fig. 11. Average converging curves of KOA, FO-KOA, ZOA, DMO, NNA, and MSA for Case 4.

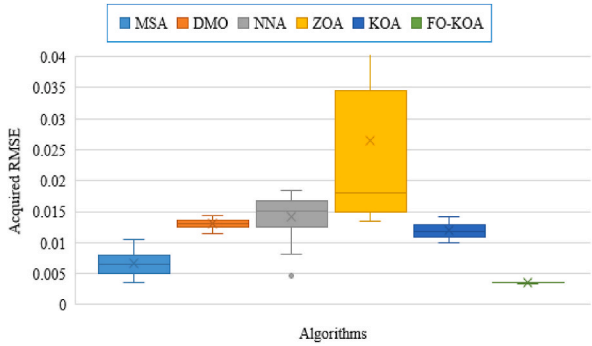

Fig. 12. FO-KOA, KOA, ZOA, DMO, NNA, and MSA boxplot of the thirty obtained RMSE objective for Case 4.

4.3.2. Case 6: application for the DDM framework (SP 70 PV module)

In this case, the proposed FO-KOA and the KOA are used to extract the DDM parameters of the SP 70 PV Module. Table 8 displays the seven unidentified DDM parameters for which each algorithm's optimal results were attained during the experiment. It can be noticed that the proposed FO-KOA obtained the best RMSE value (0.00049369), while KOA obtained the best RMSE value (0.008798587). This improvement amounts to 94.33 % of the changes in the FO-KOA that was suggested for Case 6. The results reveal that the proposed FO-KOA has excellent competitiveness in contrast to the KOA.

In Fig. 16, the convergence curves are displayed for the proposed FO-KOA, in comparison with KOA. The proposed FO-KOA obtained the best value at 670 iterations, showing that FO-KOA has more stability than KOA as well as higher precision and reliability in its comparison process for finding DDM parameters. Moreover, Fig. 17 illustrates the KOA and FO-KOA boxplot of the thirty obtained RMSE objectives for Case 6. In terms of mean RMSE, KOA exhibits a value of 0.013076276, whereas FO-KOA achieves a significantly lower mean RMSE of 0.003027345, representing a notable improvement of 76.849 %. Similarly, for maximum RMSE, KOA registers a value of 0.015919347, whereas FO-KOA achieves a lower maximum RMSE of 0.005401734, resulting in an improvement percentage of 66.068 %. Furthermore, considering the standard deviation, KOA demonstrates a value of 0.001713129, while FO-KOA exhibits a reduced standard deviation of 0.001341799, indicating a 21.676 % improvement. It can be observed from this figure that the RMSE of FO-KOA is between [1.17 E −04 to 1 E−03], whilst the RMSE of KOA is between [6 E −03 to 2 E−02]. As a result, the FO-KOA's identification of the DDM's correctness can be trusted. These findings suggest that the proposed FO-KOA algorithm outperforms KOA across all evaluated metrics, showcasing its enhanced accuracy, effectiveness, and reliability in optimizing solutions.

Fig. 18 displays the I–V curve and P–V curve of the TDM of the KC 200 PV Module that are produced from the best FO-KOA simulation settings and the actual measurement data, respectively, in order to further represent the experimental results. This figure illustrates the higher precision and reliability of the FO-KOA to obtain the current and power with different voltage levels.

4.4. Application for the RTC France cell

The suggested FO-KOA and traditional KOA approaches are used for the RTC France cell in order to extract the unknown parameters while taking the SDM (Case 7) and DDM (Case 8) into account. Regarding this, Table 9 presents the ideal parameters derived from the suggested FO-KOA and traditional KOA methodologies, in that order. Additionally, for cases 7 and 8, the related KOA and FO-KOA converging curves are shown in Fig. 19. As can be shown, for the SDM, the minimal RMSE value of 9.8602E-04 is roughly reached by both the traditional KOA and the suggested FO-KOA. In contrast, the suggested FO-KOA for the DDM obtains a lower minimum RMSE value of 9.8249E-04 compared to the traditional KOA's counterpart of 1.03737E-03. In light of this, the suggested FO-KOA outperforms the traditional KOA by 5.29 %.

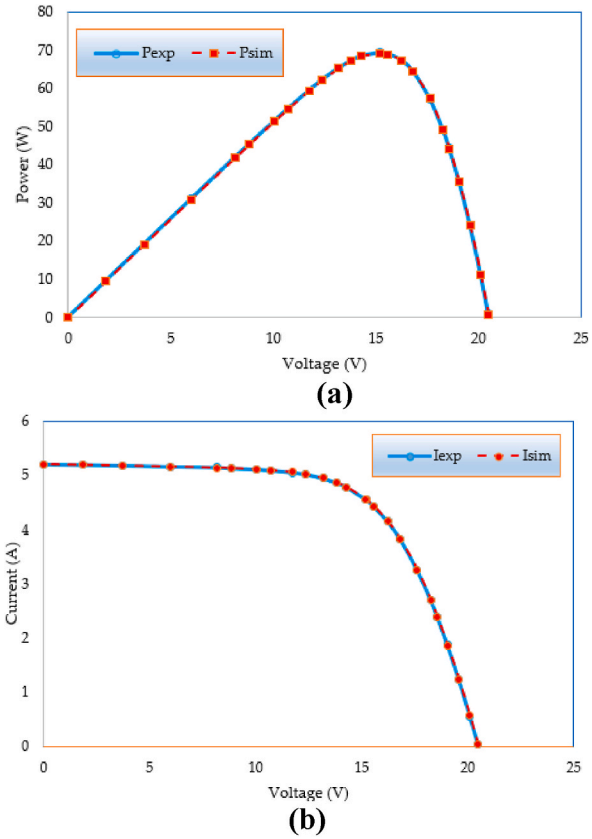

Fig. 13. (a). P–V curve based on FO-KOA for Case 4
Fig. 13(b). I–V curves based on FO-KOA for Case 4.

Table 7
Extracted Parameters based on KOA and FO-KOA for Case 5.

Item	KOA	FO-KOA
I_{ph} (A)	4.705100757	4.717085
R_s (Ω)	0.011836263	0.01260535
R_{Sh} (Ω)	4.372674058	3.46562637
I_{S1} (A)	9.48655E-08	2.2874E-08
η_1	1.307814737	1.21087793
RMSE	0.008798587	0.00049369

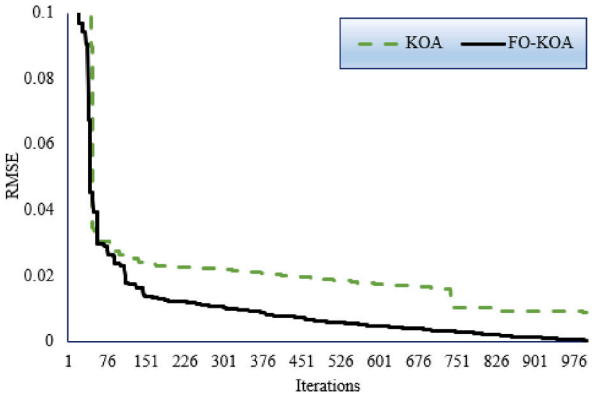

Fig. 14. FO-KOA and KOA Converging curves for Case 5.

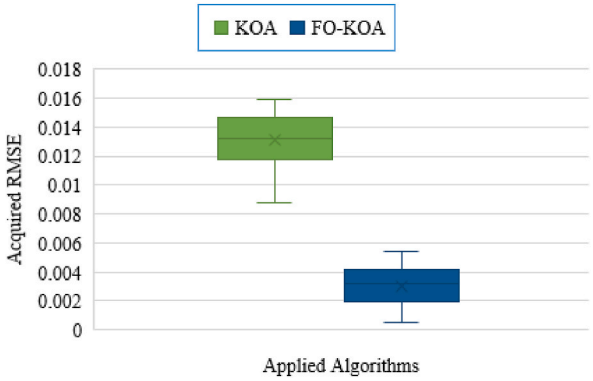

Fig. 15. FO-KOA and KOA boxplot of the thirty obtained RMSE objective for Case 5.

Table 8
Extracted Parameters based on FO-KOA and KOA for Case 6.

Item	KOA	FO-KOA
I_{ph} (A)	4.727737	4.717324
R_s (Ω)	0.012583	0.01269
R_{Sh} (Ω)	3.25975	3.454314
I_{S1} (A)	1.84E-08	5.27E-09
η_1	1.199687	1.149514
I_{S2} (A)	2.58E-07	2.95E-08
η_2	1.731166	1.297143
RMSE	0.006197	0.000117

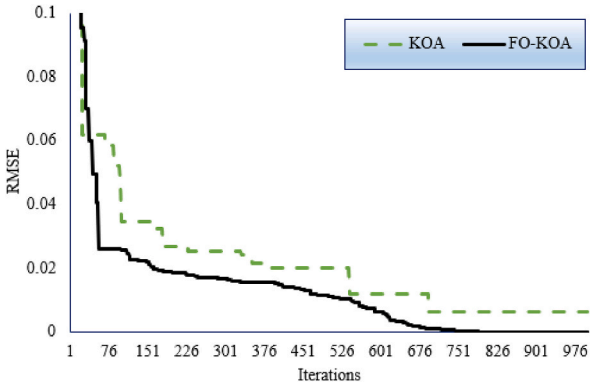

Fig. 16. KOA and FO-KOA Converging curves for Case 6.

Moreover, Fig. 20 illustrates the KOA and FO-KOA boxplot of the thirty obtained RMSE objectives for Cases 7 and 8. As shown in Fig. 20(a), in terms of the mean RMSE, KOA yields a value of 9.96192E-04, while FO-KOA demonstrates a slightly reduced mean RMSE of 9.86022E-04, representing a modest improvement of 1.02089 %. Similarly, concerning the maximum RMSE, KOA shows a value of 1.06336E-03, whereas FO-KOA achieves a notably lower maximum RMSE of 9.86022E-04, resulting in a more substantial improvement percentage of 7.27281 %. The most significant enhancement is observed in the standard deviation, where KOA presents a value of 1.55095E-05, but FO-KOA shows a substantially reduced standard deviation of 3.36377E-17, indicating a remarkable improvement of 100 %.

Similar findings are demonstrated from Fig. 20(b). For the mean RMSE, KOA records 0.001202742, while FO-KOA demonstrates a reduced mean RMSE of 0.000985042, marking an improvement of 18.100 %. Similarly, in terms of maximum RMSE, KOA shows a value of 0.00143898, whereas FO-KOA achieves a notably lower maximum RMSE of 0.000989039, resulting in an improvement percentage of 31.268 %. Noteworthy enhancements are also observed in standard deviation, with KOA presenting 0.00011956 and FO-KOA demonstrating a substantially reduced standard deviation of 1.55857E-06, indicating an impressive improvement of 98.696 %.

Fig. 17. KOA and FO-KOA boxplot of the thirty obtained RMSE objective for Case 6.

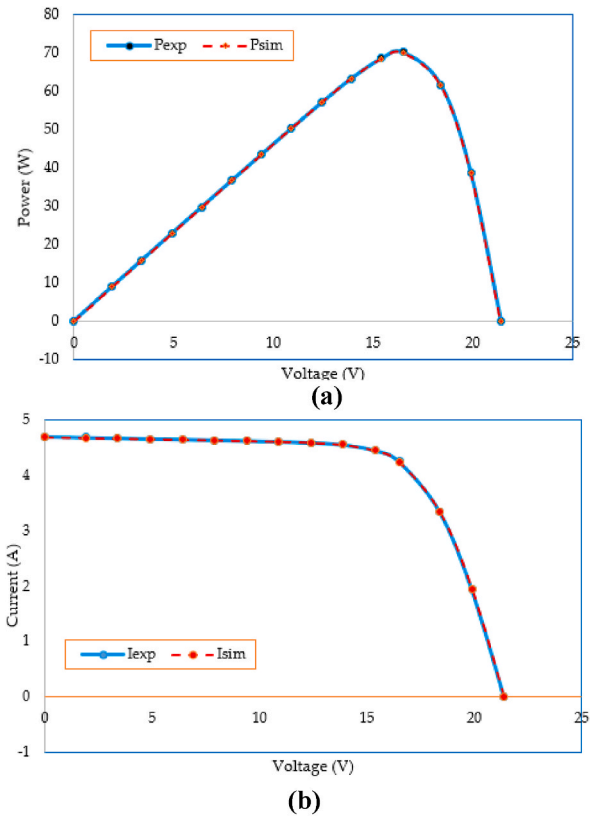

Fig. 18. (a). P–V curve based on FO-KOA for Case 6
Fig. 18(b). I–V curve based on FO-KOA for Case 6.

4.5. *Analysis of non-parametric tests: t-test and Friedman's test*

As shown previously, all the reported metrics present the FO-KOA as a promising approach for future research in this energy-saving optimization problem. In this section, the study is extended with the analysis of non-parametric tests considering the *t*-test and the Friedman's test. For this purpose, the Ultra Power 85 PV module is considered via both models: the SDM (Case 3) and the DDM (Case 4). For both models, the *t*-test is executed for comparing the proposed FO-KOA from one side and each other algorithm (MSA, DMO, NNA, ZOA and KOA) in the other side as a two-sample *t*-test. The MATLAB results of the *t*-test are tabulated in Tables 10 and 11, respectively for both models. As shown, the h-value is always unity and the p-value is always a very small number, indicating that the null hypothesis can be rejected. For instance, the smallest p-value is 3.02E-43, indicating an extremely low probability of observing such extreme results if the null hypothesis were true. Also, larger absolute values of t-statistic measures indicate a greater difference

Table 9
Validation of the proposed FO-KOA on SDM and DDM of the RTC France PV Cell.

Item	Case 7 (SDM)		Case 8 (DDM)	
	KOA	FO-KOA	KOA	FO-KOA
I_{ph} (A)	0.760775656	0.76077553	0.760574616	0.76078159
R_s (Ω)	0.036377574	0.036377093	0.035743299	0.036738323
R_{Sh} (Ω)	53.71496384	53.71852199	58.78462724	55.49340792
I_{S1} (A)	3.22942E-07	3.23021E-07	6.33675E-08	2.26117E-07
η_1	1.481158728	1.481183586	1.971851075	1.451076506
I_{S2} (A)	–	–	3.61845E-07	7.49178E-07
η_2	–	–	1.493213083	2
RMSE	9.86023E-04	9.860218E-04	1.03737E-03	9.8249E-04

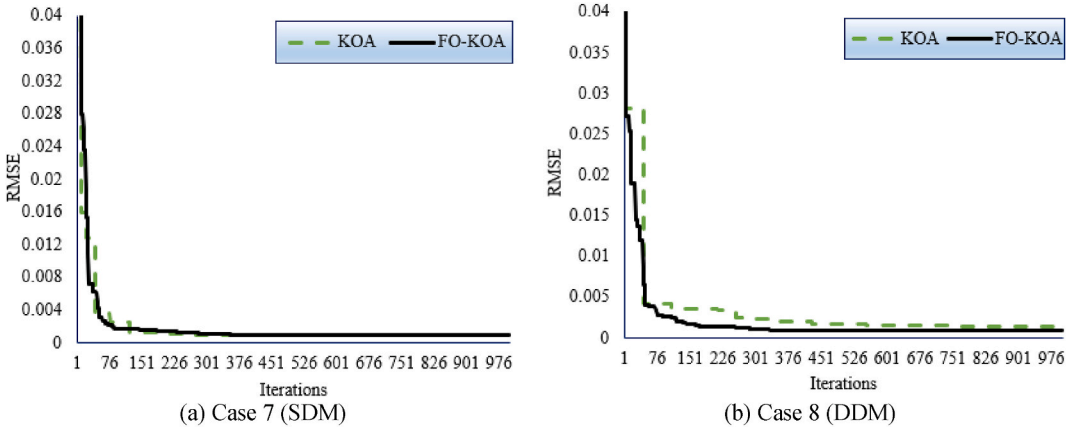

Fig. 19. KOA and FO-KOA Converging curves for Cases 7 and 8.

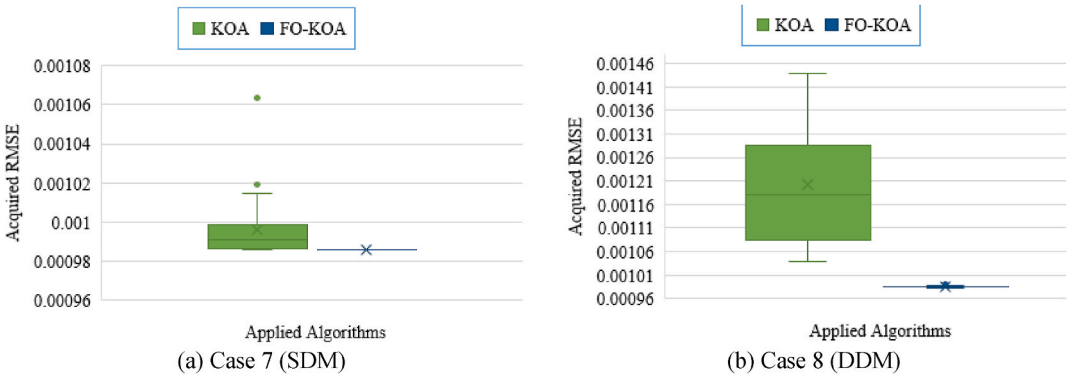

Fig. 20. KOA and FO-KOA boxplot of the thirty obtained RMSE objective for Cases 7 and 8.

Table 10
Results of *t*-test on SDM of the Ultra Power 85 PV module.

	FO-KOA vs MSA	FO-KOA vs DMO	FO-KOA vs NNA	FO-KOA vs ZOA	FO-KOA vs KOA
h	1	1	1	1	1
p	1.65E-05	3.02E-43	8.54E-14	3.00E-12	4.66E-23
ci	−0.0001986	−0.0065	−0.0093	−0.0245	−0.0033
	−0.0000799	−0.0059	−0.0061	−0.0154	−0.0026
tstat	−4.6984	−38.8923	−9.7280	−8.7856	−16.0939
df	58	58	58	58	58
sd	1.1482E-4	6.1659E-4	0.0031	0.0088	7.0739E-4

Table 11
Results of *t*-test on DDM of the Ultra Power 85 PV module.

	FO-KOA vs MSA	FO-KOA vs DMO	FO-KOA vs NNA	FO-KOA vs ZOA	FO-KOA vs KOA
h	1	1	1	1	1
p	2.41E-13	1.05E-59	6.79E-26	2.01E-09	1.21E-43
ci	−0.0037	−0.0098	−0.0119	−0.0293	−0.0089
	−0.0024	−0.0093	−0.0096	−0.0164	−0.008
tstat	−9.4514	−75.7683	−18.4067	−7.0975	−39.5354
df	58	58	58	58	58
sd	0.0013	4.8961E-4	0.0023	0.0125	8.3013E-4

between the algorithms being compared. For example, a t-statistic of −38.8923 in the comparison FO-KOA vs MSA suggests a substantial difference in standard deviations between them. Moreover, the degrees of freedom (*df*) are all 58, suggesting a reasonably large sample size for each comparison.

Also, Friedman's test is executed for the SDM and the regarding table is tabulated in Table 12. In this table, the columns' source of variation is listed as "Columns," indicating the variability among different algorithms. The high chi-square value (158.9) and very low probability (1.69453E-32) suggest that there are statistically significant differences among the algorithms in terms of SDM.

Similar to Table 12, Table 13 presents the results of Friedman's ANOVA, but for DDM. The chi-square value (157.18) and the associated probability (3.95785E-32) suggest statistically significant differences among the algorithms in terms of DDM.

In summary, both tests indicate that there are statistically significant differences among the algorthims concerning SDM and DDM of the Ultra Power 85 PV module.

4.6. Computational complexity and runtime: FO-KOA versus KOA in solving PV cell parameters extraction

A computational complexity analysis for the algorithmic methods can be carried out using the "Big O analysis" [66]. The execution times of the techniques were determined for comparison purposes. In the beginning the number of the initial solution options is specified as N_S, and d is the dimension of the PV cell parameters extraction problem under discussion. In the KOA and FO-KOA searching process, the computational complexity of addressing each solution individual's information in the search space is O($T_{\max}\bigtimes N_S\bigtimes d$). Therefore, O($T_{\max}\bigtimes N_S\bigtimes d$) $\bigtimes$O(*fitness(x)*) represents the computational complexity of the objective function assessment in the KOA and FO-KOA. Upon careful consideration, Table 14 provides a comprehensive overview of the computational complexities observed across each case study. Notably, the transition from handling the SDM to the DDM in the PV cell characteristics extraction problem introduces a notable escalation in computational complexity, marked by a 28.57 % increase as the dimension expands. This uptick underscores the intensified computational demands associated with processing higher-dimensional data. Moreover, the original KOA provides slightly smaller run time than the proposed FO-KOA with additional fractional order component.

5. Conclusions

A revolutionary enhanced Fractional Order Kepler optimization algorithm (FO-KOA) is introduced for the first time in this paper. The algorithm's performance is enhanced by the method using the ideas of FO to enhance the diversity and speed of intelligence and LEA to find better solutions by searching more thoroughly for high-quality solution solutions in local areas. The proposed FO-KOA is identified for the KC-200 PV module, SP-70 and the Ul-tra-Power-85 PV modules features in solar systems. The proposed FO-KOA has a significant advantage and robustness over earlier reported results for both PV modules. Six case studies are elaborated in this study to show the ability of the proposed FO-KOA to obtain the PV cell parameters. The SDM and DDM test the algorithm's effectiveness, where there is an excellent match between the simulated and real data. For the KC 200 PV Module, the proposed FO-KOA technique shows improvements to 94.43 % and 96.65 % compared to KOA for Cases 1 and 2, respectively. Furthermore, for the Ultra Power 85 PV Module, the proposed FO-KOA shows improvement with 3.762 %, 63.473 %, 68.373 %, 84.846 % and 45.205 %, respectively compared to MSA, DMO, NNA, ZOA and KOA for Case 3. Also, it shows improvement with 46.062 %, 72.764 %, 74.956 %, 86.487 % and 74.758 % for Case 4. Additionally, for the *SP* 70 PV Module, the proposed FO-KOA technique shows improvements to 94.38 % and 96.33 % compared to KOA for Cases 5 and 6, respectively. The convergence curves and the boxplot analysis show that FO-KOA has more stability than KOA as well as higher precision and reliability in its comparison process for finding parameters.

Based on the above, the proposed FO-KOA algorithm shows several advantages in identifying the parameters of the PV systems. However, some limitations are required to be handled. Like many optimization algorithms, FO-KOA's performance may be sensitive to

Table 12
Friedman's ANOVA Table on SDM of the Ultra Power 85 PV module.

Source	SS	df	MS	Chi-sq	Prob > Chi-sq
Columns	17558.9	5	3511.79	158.9	1.69453E-32
Interaction	1069.1	20	53.45		
Error	709.5	150	4.73		
Total	19337.5	179			

Table 13
Friedman's ANOVA Table on DDM of the Ultra Power 85 PV module.

Source	SS	df	MS	Chi-sq	Prob > Chi-sq
Columns	17446.5	5	3489.29	157.18	3.95785E-32
Interaction	806.5	20	40.33		
Error	1172	150	7.81		
Total	19425	179			

Table 14
Computational complexity and runtime of KOA and FO-KOA on DDM of the Ultra Power 85 PV module.

	N_S	T_{max}	Dimension and Computational complexity			Average Runtime (Seconds)/Iteration		
KC200GT	100	1000		d	Computational complexity		KOA	FO-KOA
			Case 1	5	O(500,000)	Case 1	0.0462	0.0534
			Case 2	7	O(700,000)	Case 2	0.466	0.0541
Ultra 85-P PV	100	300		d	Computational complexity		KOA	FO-KOA
			Case 3	5	O(500,000)	Case 3	0.0467	0.0519
			Case 4	7	O(700,000)	Case 4	0.0486	0.0558
SP70 PV	100	1000		d	Computational complexity		KOA	FO-KOA
			Case 5	5	O(500,000)	Case 5	0.0469	0.0522
			Case 6	7	O(700,000)	Case 6	0.0485	0.0562
RTC France cell	100	1000		d	Computational complexity		KOA	FO-KOA
			Case 7	5	O(500,000)	Case 7	0.0462	0.0514
			Case 8	7	O(700,000)	Case 8	0.0551	0.0555

the initial values of its parameters. While FO-KOA demonstrates efficient convergence in our experiments, further research applications are warranted to examine its performance in other engineering problems. FO-KOA has been successfully designed and tested extensively in the context of PV parameter extraction considering SDM and DDM. It is recommended, as a future work, to investigate the FO-KOA's performance for more complex equivalent circuits such as the triple diode model.

Data availability statement

Data included in article/supp. material/referenced in the article is available.

CRediT authorship contribution statement

Sultan Hassan Hakmi: Writing – review & editing, Supervision. **Hashim Alnami:** Investigation, Formal analysis, Data curation. **Ahmed Ginidi:** Writing – original draft, Methodology, Conceptualization. **Abdullah Shaheen:** Writing – original draft, Software, Conceptualization. **Thamer A.H. Alghamdi:** Writing – review & editing, Validation, Investigation.

Declaration of competing interest

The authors declare that they have no known competing financial interests or personal relationships that could have appeared to influence the work reported in this paper.

Acknowledgments

The authors extend their appreciation to the Deputyship for Research & Innovation, Ministry of Education in Saudi Arabia for funding this research work through the project number ISP23-122.

References

[1] S.O. Ayanlade, et al., Optimal allocation of photovoltaic distributed generations in radial distribution networks, Sustainability 15 (18) (Sep. 2023) 13933, https://doi.org/10.3390/su151813933.
[2] S.M. Ebrahimi, E. Salahshour, M. Malekzadeh, Francisco Gordillo, Parameters identification of PV solar cells and modules using flexible particle swarm optimization algorithm, Energy 179 (2019) 358–372, https://doi.org/10.1016/j.energy.2019.04.218.
[3] X. Chen, K. Yu, W. Du, W. Zhao, G. Liu, Parameters identification of solar cell models using generalized oppositional teaching learning based optimization, Energy 99 (2016) 170–180, https://doi.org/10.1016/j.energy.2016.01.052.
[4] Rizk M. Rizk-Allah, A.A. El-Fergany, Emended heap-based optimizer for characterizing performance of industrial solar generating units using triple-diode model, Energy 237 (2021) 121561.
[5] T. Easwarakhanthan, J. Bottin, I. Bouhouch, C. Boutrit, Nonlinear minimization algorithm for determining the solar cell parameters with microcomputers, Int. J. Sol. Energy 4 (1) (1986) 1–12, https://doi.org/10.1080/01425918608909835.
[6] A. Ortiz-Conde, F.J. García Sánchez, J. Muci, New method to extract the model parameters of solar cells from the explicit analytic solutions of their illuminated I–V characteristics, Sol. Energy Mater. Sol. Cells 90 (3) (Feb. 2006) 352–361, https://doi.org/10.1016/J.SOLMAT.2005.04.023.

[7] Y. Fan, P. Wang, M. Mafarja, M. Wang, X. Zhao, H. Chen, A bioinformatic variant fruit fly optimizer for tackling optimization problems, Knowl. Base Syst. 213 (2021), https://doi.org/10.1016/j.knosys.2020.106704.

[8] M.M. Alam, T. Alshahrani, F. Khan, J. Hakami, S.M. Shinde, R. Azim, AI-based efficiency analysis technique for photovoltaic renewable energy system, Phys. Scripta 98 (12) (Dec. 2023) 126006, https://doi.org/10.1088/1402-4896/ad0bb4.

[9] E.S. Ali, S.M. Abd Elazim, S.H. Hakmi, M.I. Mosaad, Optimal allocation and size of renewable energy sources as distributed generations using shark optimization algorithm in radial distribution systems, Energies 16 (10) (May 2023) 3983, https://doi.org/10.3390/en16103983.

[10] I.H. Smaili, D.R. Almalawi, A.M. Shaheen, H.S.E. Mansour, Optimizing PV sources and shunt capacitors for energy efficiency improvement in distribution systems using subtraction-average algorithm, Mathesis 12 (2024) 625, https://doi.org/10.3390/MATH12050625, vol. 12, no. 5, p. 625, Feb. 2024.

[11] Z. Alaas, Z.M.S. Elbarbary, A. Rezvani, B.N. Le, M. khaki, Analysis and enhancement of MPPT technique to increase accuracy and speed in photovoltaic systems under different conditions, Optik 289 (Oct. 2023) 171208, https://doi.org/10.1016/J.IJLEO.2023.171208.

[12] H.M. Ridha, A.A. Heidari, M. Wang, H. Chen, Boosted mutation-based Harris hawks optimizer for parameters identification of single-diode solar cell models, Energy Convers. Manag. 209 (Apr. 2020) 112660, https://doi.org/10.1016/J.ENCONMAN.2020.112660.

[13] H. Chen, S. Jiao, M. Wang, A.A. Heidari, X. Zhao, Parameters identification of photovoltaic cells and modules using diversification-enriched Harris hawks optimization with chaotic drifts, J. Clean. Prod. 244 (Jan. 2020) 118778, https://doi.org/10.1016/j.jclepro.2019.118778.

[14] H. Zhang, A.A. Heidari, M. Wang, L. Zhang, H. Chen, C. Li, Orthogonal Nelder-Mead moth flame method for parameters identification of photovoltaic modules, Energy Convers. Manag. 211 (May 2020) 112764, https://doi.org/10.1016/J.ENCONMAN.2020.112764.

[15] Y. Liu, et al., Horizontal and vertical crossover of Harris hawk optimizer with Nelder-Mead simplex for parameter estimation of photovoltaic models, Energy Convers. Manag. 223 (Nov. 2020) 113211, https://doi.org/10.1016/J.ENCONMAN.2020.113211.

[16] H. Chen, S. Jiao, A.A. Heidari, M. Wang, X. Chen, X. Zhao, An opposition-based sine cosine approach with local search for parameter estimation of photovoltaic models, Energy Convers. Manag. 195 (Sep. 2019) 927–942, https://doi.org/10.1016/J.ENCONMAN.2019.05.057.

[17] Z. Wu, D. Yu, X. Kang, Parameter identification of photovoltaic cell model based on improved ant lion optimizer, Energy Convers. Manag. 151 (Nov. 2017) 107–115, https://doi.org/10.1016/J.ENCONMAN.2017.08.088.

[18] F.F. Liu, S.C. Chu, C.C. Hu, J. Watada, J.S. Pan, An effective QUATRE algorithm based on reorganized mechanism and its application for parameter estimation in improved photovoltaic module, Heliyon 9 (6) (2023) e16468, https://doi.org/10.1016/j.heliyon.2023.e16468.

[19] P.J. Gnetchejo, S. Ndjakomo Essiane, A. Dadjé, P. Ele, A combination of Newton-Raphson method and heuristics algorithms for parameter estimation in photovoltaic modules, Heliyon 7 (4) (Apr. 2021) e06673, https://doi.org/10.1016/J.HELIYON.2021.E06673.

[20] D. Maden, E. Çelik, E.H. Houssein, G. Sharma, Squirrel search algorithm applied to effective estimation of solar PV model parameters: a real-world practice, Neural Comput. Appl. 35 (18) (2023), https://doi.org/10.1007/s00521-023-08451-x.

[21] Z. Garip, Parameters estimation of three-diode photovoltaic model using fractional-order Harris Hawks optimization algorithm, Optik 272 (2023), https://doi.org/10.1016/j.ijleo.2022.170391.

[22] A. Elkholy, A.A. Abou El-Ela, Optimal parameters estimation and modelling of photovoltaic modules using analytical method, Heliyon 5 (7) (2019) e02137, https://doi.org/10.1016/j.heliyon.2019.e02137.

[23] M. Qaraad, S. Amjad, N.K. Hussein, M. Badawy, S. Mirjalili, M.A. Elhosseini, Photovoltaic parameter estimation using improved moth flame algorithms with local escape operators, Comput. Electr. Eng. 106 (2023), https://doi.org/10.1016/j.compeleceng.2023.108603.

[24] M. Qaraad, S. Amjad, N.K. Hussein, M.A. Farag, S. Mirjalili, M.A. Elhosseini, Quadratic interpolation and a new local search approach to improve particle swarm optimization: solar photovoltaic parameter estimation, Expert Syst. Appl. 236 (2024), https://doi.org/10.1016/j.eswa.2023.121417.

[25] H.G.G. Nunes, J.A.N. Pombo, S.J.P.S. Mariano, M.R.A. Calado, J.A.M. Felippe de Souza, A new high performance method for determining the parameters of PV cells and modules based on guaranteed convergence particle swarm optimization, Appl. Energy 211 (November 2017) (2018) 774–791, https://doi.org/10.1016/j.apenergy.2017.11.078.

[26] M. Merchaoui, A. Sakly, M.F. Mimouni, Particle swarm optimisation with adaptive mutation strategy for photovoltaic solar cell/module parameter extraction, Energy Convers. Manag. 175 (Nov. 2018) 151–163, https://doi.org/10.1016/J.ENCONMAN.2018.08.081.

[27] S. Jiao, et al., Orthogonally adapted Harris hawks optimization for parameter estimation of photovoltaic models, Energy 203 (2020) 117804, https://doi.org/10.1016/j.energy.2020.117804.

[28] H.M. Ridha, C. Gomes, H. Hizam, M. Ahmadipour, A.A. Heidari, H. Chen, Multi-objective optimization and multi-criteria decision-making methods for optimal design of standalone photovoltaic system: a comprehensive review, Renew. Sustain. Energy Rev. 135 (Jan. 2021) 110202, https://doi.org/10.1016/J.RSER.2020.110202.

[29] A. Abbassi, et al., Parameters identification of photovoltaic cell models using enhanced exploratory salp chains-based approach, Energy 198 (2020) 117333, https://doi.org/10.1016/j.energy.2020.117333.

[30] M. Abdel-Basset, R. Mohamed, S.A.A. Azeem, M. Jameel, M. Abouhawwash, Kepler optimization algorithm: a new metaheuristic algorithm inspired by Kepler's laws of planetary motion, Knowl. Base Syst. 268 (May 2023) 110454, https://doi.org/10.1016/J.KNOSYS.2023.110454.

[31] S.H. Hakmi, A.M. Shaheen, H. Alnami, G. Moustafa, A. Ginidi, Kepler algorithm for large-scale systems of economic dispatch with heat optimization, Biomimetics 8 (8) (Dec. 2023) 608, https://doi.org/10.3390/biomimetics8080608.

[32] A.M. Shaheen, R.A. El-Sehiemy, A. Ginidi, A.M. Elsayed, S.F. Al-Gahtani, Optimal allocation of PV-STATCOM devices in distribution systems for energy losses minimization and voltage profile improvement via hunter-prey-based algorithm, Energies 16 (6) (Mar. 2023) 2790, https://doi.org/10.3390/en16062790.

[33] X. Yu, Y. Duan, Z. Cai, Sub-population improved grey wolf optimizer with Gaussian mutation and Lévy flight for parameters identification of photovoltaic models, Expert Syst. Appl. 232 (Dec. 2023) 120827, https://doi.org/10.1016/J.ESWA.2023.120827.

[34] V.J. Chin, Z. Salam, K. Ishaque, Cell modelling and model parameters estimation techniques for photovoltaic simulator application: a review, Appl. Energy 154 (2015) 500–519, https://doi.org/10.1016/j.apenergy.2015.05.035.

[35] A.R. Ginidi, A.M. Shaheen, R.A. El-Sehiemy, H.M. Hasanien, A. Al-Durra, Estimation of electrical parameters of photovoltaic panels using heap-based algorithm, IET Renew. Power Gener. 16 (11) (Aug. 2022) 2292–2312, https://doi.org/10.1049/RPG2.12523.

[36] A.M. Shaheen, A.M. Elsayed, A.R. Ginidi, R.A. El-Sehiemy, E. Elattar, Enhanced social network search algorithm with powerful exploitation strategy for PV parameters estimation, Energy Sci. Eng. 10 (4) (2022) 1398–1417, https://doi.org/10.1002/ese3.1109.

[37] M. Elshahed, A.M. El-Rifaie, M.A. Tolba, A. Ginidi, A. Shaheen, S.A. Mohamed, An innovative hunter-prey-based optimization for electrically based single-, double-, and triple-diode models of solar photovoltaic systems, Mathematics 10 (23) (Dec. 2022) 4625, https://doi.org/10.3390/math10234625.

[38] H. Ben Aribia, et al., Growth optimizer for parameter identification of solar photovoltaic cells and modules, Sustainability 15 (10) (May 2023) 7896, https://doi.org/10.3390/su15107896.

[39] Y. Lu, S. Liang, H. Ouyang, S. Li, G. ge Wang, Hybrid multi-group stochastic cooperative particle swarm optimization algorithm and its application to the photovoltaic parameter identification problem, Energy Rep. 9 (Dec. 2023) 4654–4681, https://doi.org/10.1016/J.EGYR.2023.03.105.

[40] V.J. Chin, Z. Salam, Coyote optimization algorithm for the parameter extraction of photovoltaic cells, Sol. Energy 194 (2019) 656–670, https://doi.org/10.1016/j.solener.2019.10.093.

[41] O.S. Elazab, H.M. Hasanien, I. Alsaidan, A.Y. Abdelaziz, S.M. Muyeen, Parameter estimation of three diode photovoltaic model using grasshopper optimization algorithm, Energies 13 (2) (2020), https://doi.org/10.3390/en13020497.

[42] G. Moustafa, M. Elshahed, A.R. Ginidi, A.M. Shaheen, H.S.E. Mansour, A gradient-based optimizer with a crossover operator for distribution static VAR compensator (D-SVC) sizing and placement in electrical systems, Mathematics 11 (5) (Feb. 2023) 1077, https://doi.org/10.3390/math11051077.

[43] D. Yousri, M. Abd Elaziz, D. Oliva, A. Abraham, M.A. Alotaibi, M.A. Hossain, Fractional-order comprehensive learning marine predators algorithm for global optimization and feature selection, Knowl. Base Syst. 235 (Jan. 2022) 107603, https://doi.org/10.1016/J.KNOSYS.2021.107603.

[44] Shell PowerMax solar modules for off-grids markets, Shell Solar, The Hague. http://www.effectivesolar.com/PDF/shell/SQ-80-85-P.pdf, 2019.

[45] R. El-Sehiemy, A. Shaheen, A. El-Fergany, A. Ginidi, Electrical parameters extraction of PV modules using artificial hummingbird optimizer, Sci. Rep. 13 (9240) (2023), https://doi.org/10.1038/s41598-023-36284-0.

[46] A. Ginidi, S.M. Ghoneim, A. Elsayed, R. El-Sehiemy, A. Shaheen, A. El-Fergany, Gorilla troops optimizer for electrically based single and double-diode models of solar photovoltaic systems, Sustainability 13 (2021) 9459, https://doi.org/10.3390/su13169459.
[47] K. Yu, B. Qu, C. Yue, S. Ge, X. Chen, J. Liang, A performance-guided JAYA algorithm for parameters identification of photovoltaic cell and module, Appl. Energy 237 (2019) 241–257, https://doi.org/10.1016/j.apenergy.2019.01.008.
[48] E.E. Ali, M.A. El-Hameed, A.A. El-Fergany, M.M. El-Arini, Parameter extraction of photovoltaic generating units using multi-verse optimizer, Sustain. Energy Technol. Assessments 17 (2016) 68–76, https://doi.org/10.1016/j.seta.2016.08.004.
[49] R.M. Rizk-Allah, A.A. El-Fergany, Conscious neighborhood scheme-based Laplacian barnacles mating algorithm for parameters optimization of photovoltaic single- and double-diode models, Energy Convers. Manag. 226 (June) (2020) 113522, https://doi.org/10.1016/j.enconman.2020.113522.
[50] A.M. Shaheen, A.R. Ginidi, R.A. El-Sehiemy, S.S.M. Ghoneim, A forensic-based investigation algorithm for parameter extraction of solar cell models, IEEE Access 9 (2021) 1–20, https://doi.org/10.1109/ACCESS.2020.3046536.
[51] A.M. Beigi, A. Maroosi, Parameter identification for solar cells and module using a hybrid firefly and pattern search algorithms, Sol. Energy 171 (2018) 435–446, https://doi.org/10.1016/j.solener.2018.06.092.
[52] V. Khanna, B.K. Das, D. Bisht, Vandana, P.K. Singh, A three diode model for industrial solar cells and estimation of solar cell parameters using PSO algorithm, Renew. Energy 78 (2015) 105–113, https://doi.org/10.1016/j.renene.2014.12.072.
[53] M.H. Sulaiman, Z. Mustaffa, M.M. Saari, H. Daniyal, Barnacles Mating Optimizer: a new bio-inspired algorithm for solving engineering optimization problems, Eng. Appl. Artif. Intell. 87 (2020), https://doi.org/10.1016/j.engappai.2019.103330.
[54] A.F. Nematollahi, A. Rahiminejad, B. Vahidi, A novel physical based meta-heuristic optimization method known as Lightning Attachment Procedure Optimization, Appl. Soft Comput. J. 59 (2017) 596–621, https://doi.org/10.1016/j.asoc.2017.06.033.
[55] J. Liang, et al., Classified perturbation mutation based particle swarm optimization algorithm for parameters extraction of photovoltaic models, Energy Convers. Manag. 203 (June 2019) (2020) 112138, https://doi.org/10.1016/j.enconman.2019.112138.
[56] G. Kanimozhi, Harish Kumar, Modeling of solar cell under different conditions by Ant Lion Optimizer with LambertW function, Appl. Soft Comput. J. 71 (2018) 141–151, https://doi.org/10.1016/j.asoc.2018.06.025.
[57] H. Ben Aribia, et al., Growth optimizer for parameter identification of solar photovoltaic cells and modules, Sustainability 15 (10) (May 2023) 7896, https://doi.org/10.3390/su15107896.
[58] F.A. Şenel, F. Gökçe, A.S. Yüksel, T. Yiğit, A novel hybrid PSO–GWO algorithm for optimization problems, Eng. Comput. 35 (4) (Oct. 2019) 1359–1373, https://doi.org/10.1007/s00366-018-0668-5.
[59] J.O. Agushaka, A.E. Ezugwu, L. Abualigah, Dwarf mongoose optimization algorithm, Comput. Methods Appl. Mech. Eng. 391 (2022), https://doi.org/10.1016/j.cma.2022.114570.
[60] G. Moustafa, et al., An enhanced dwarf mongoose optimization algorithm for solving engineering problems, Mathematics 11 (15) (Jul. 2023) 3297, https://doi.org/10.3390/math11153297.
[61] G. Moustafa, et al., Dwarf mongoose optimizer for optimal modeling of solar PV systems and parameter extraction, Electronics 12 (24) (Dec. 2023) 4990, https://doi.org/10.3390/electronics12244990.
[62] H. Alnami, A.M. El-Rifaie, G. Moustafa, S.H. Hakmi, A.M. Shaheen, M.A. Tolba, Optimal allocation of TCSC devices in transmission power systems by a novel adaptive dwarf mongoose optimization, IEEE Access (Dec. 2023) 1, https://doi.org/10.1109/ACCESS.2023.3346533, 1.
[63] A. Sadollah, H. Sayyaadi, A. Yadav, A dynamic metaheuristic optimization model inspired by biological nervous systems: neural network algorithm, Appl. Soft Comput. J. 71 (2018), https://doi.org/10.1016/j.asoc.2018.07.039.
[64] E. Trojovska, M. Dehghani, P. Trojovsky, Zebra optimization algorithm: a new bio-inspired optimization algorithm for solving optimization algorithm, IEEE Access 10 (2022), https://doi.org/10.1109/ACCESS.2022.3172789.
[65] G. Moustafa, H. Alnami, S.H. Hakmi, A. Ginidi, A.M. Shaheen, F.A. Al-Mufadi, An advanced bio-inspired Mantis search algorithm for characterization of PV panel and global optimization of its model parameters, Biomimetics 8 (6) (Oct. 2023) 490, https://doi.org/10.3390/BIOMIMETICS8060490, 2023, Vol. 8, Page 490.
[66] S. Sarhan, R.A. El-Sehiemy, A.M. Shaheen, M. Gafar, TLBO merged with studying effect for economic environmental energy management in high voltage AC networks hybridized with multi-terminal DC lines, Appl. Soft Comput. 143 (Aug. 2023) 110426, https://doi.org/10.1016/J.ASOC.2023.110426.